Perturbing HIV-1 genomic RNA subcellular localization inhibits virus particle production

Jordan T. Becker & Nathan M. Sherer

McArdle Laboratory for Cancer Research, Institute for Molecular Virology, & Carbone Cancer Center
University of Wisconsin – Madison
1525 Linden Drive, Madison, WI 53706

Short title: HIV-1 gRNA localization regulates virion production

*To whom correspondence should be addressed: 501 Robert M. Bock Lab, 1525 Linden Drive, Madison, WI 53706. Tel: (608) 890-2551. Email: nsherer@wisc.edu

Abstract. mRNA subcellular localization is a crucial determinant of eukaryotic gene expression. For retroviruses including HIV-1, the unspliced genomic RNA (gRNA) serves both as the mRNA encoding Gag/Gag-Pol capsid proteins and the genetic material packaged by Gag into virions assembling at the plasma membrane. Gag is sufficient to drive the assembly of virus-like particles in the absence of gRNA binding. Thus, what role gRNA cytoplasmic trafficking plays during assembly is unknown. Here we demonstrate that aberrantly tethering HIV-1 gRNAs to membranes or the actin cytoskeleton alters Gag subcellular distribution and reduces virus particle production. This block was restricted to gRNAs competent for Gag synthesis and mapped to the Rev response element; a *cis*-acting RNA structure that regulates gRNA nuclear export. These results expose an unexpected mechanistic link between HIV-1 gRNA nuclear history, cytoplasmic trafficking, and Gag assembly. Perturbing viral mRNA subcellular distribution could represent a novel antiviral strategy.

INTRODUCTION

The spatial distribution of messenger RNAs (mRNAs) within the cell is a core determinant of mRNA turnover, cytoplasmic utilization, and often the formation of functional macromolecular complexes (1–5). Viruses face severe challenges in this regard during the productive phases of infection, wherein viral mRNAs, genomes, and core structural elements must be compartmentalized in space and time to form and release infectious virions. For the human immunodeficiency virus type 1 (HIV-1), virion assembly occurs at the plasma membrane (PM) (6) where a dimer of ~9kb, unspliced genomic RNA (gRNA) is encapsidated into enveloped, proteinaceous shells consisting of ~2,000 Gag (and Gag-Pol) capsid polyproteins (7, 8). Upstream of assembly, Gag/Gag-Pol and gRNAs orchestrate an elegant interplay with gRNAs functioning both as mRNAs encoding Gag and Gag-Pol as well as the core genetic substrate bound by Gag and trafficked to the site of assembly (9–12). Curiously, Gag is sufficient to drive the assembly of virus-like particles (VLPs) even in the absence of gRNA binding (13–17). As such, how Gag/gRNA trafficking behaviors in the cytoplasm are coordinated for efficient assembly and encapsidation is poorly understood.

To initiate assembly, Gag requires association with the PM via a phospholipid membrane anchor and must also interact with an RNA scaffold in the cytoplasm (16, 18, 19). Four functional domains of the Gag polyprotein coordinate this process. Matrix (MA) targets Gag to the cytosolic face of the PM through interactions with the phospholipid phosphatidylinositol 4,5-bisphosphate ($PI(4,5)P_2$) (20–23). Capsid (CA) coordinates Gag-Gag interactions during capsid assembly (24, 25). NC binds to the

gRNA dimer and/or cellular RNA (26–29) and the p6 “late” domain recruits the cellular endosomal sorting complex required for transport (ESCRT) machinery that catalyzes membrane abscission and particle release (15, 30–33). Under infectious conditions, Gag encapsidates a gRNA dimer with high efficiency (34–36) through NC’s binding to a *cis*-acting RNA packaging signal known as Psi located in the gRNA’s 5’ untranslated region (29, 37–39). NC also binds to cellular RNAs and can package some highly structured RNAs (*e.g.*, U6 snRNAs and 7SL RNAs) into virions with a high degree of specificity (40–43). Interestingly, MA can also bind to RNAs (in particular, cellular tRNAs) (39, 44–46), an activity that may regulate MA-membrane interactions and thus affect assembly (45, 46).

Gag and gRNAs are coordinately trafficked to sites of assembly in the form of dynamic viral genomic ribonucleoprotein (gRNP) complexes consisting of HIV-1 gRNAs bound to low-order multiples of Gag and cellular RNA binding proteins (47–49). gRNP trafficking complexes likely form in conjunction with nuclear export and can traffic to PM assembly sites via diffusion (50). However, membrane trafficking and/or the cytoskeleton have also been implicated in gRNP cytoplasmic trafficking in some studies (51–53). Particle assembly is initiated when cytoplasmic Gag concentrations reach a critical level, the so-called cooperative threshold (54) wherein Gag-Gag interactions trigger the activation of a myristoyl switch within MA that subsequently anchors the gRNP complex to the PM (21, 55–57). Recent imaging studies suggest that this event occurs in concert with or just prior to gRNA dimerization (58) and is followed by the gradual recruitment of Gag molecules to the assembling virion over 10-30 minutes (36, 59–62).

Although Gag-gRNA binding is not obligatory for assembly (63–65), we and others have provided evidence for important functional links between gRNA nucleocytoplasmic trafficking and Gag's assembly competency (66–69). Retroviral gRNAs retain introns and have evolved to hijack specialized cellular RNA nuclear export machineries (70–72). HIV-1 gRNAs are exported from the nucleus through an interaction between the cellular karyopherin CRM1, the viral Rev protein, and a *cis*-acting RNA secondary structure, the Rev-response element (RRE) found in gRNAs and a subset of incompletely spliced transcripts that encode the viral Vif, Vpu, and Envelope proteins (73–75). Genetically simpler retroviruses lack Rev-equivalent proteins and instead encode *cis*-acting RNA constitutive transport elements (CTEs) that are CRM1-independent and directly recruit the NXF1(TAP)/NXT1(p15) mRNA nuclear export machinery, similar to the bulk of cellular spliced mRNAs (76–80). Rendering HIV-1 gRNAs or surrogate *gag-pol* mRNAs Rev-independent (*e.g.,* by replacing the RRE with one or more CTEs or by codon-optimizing the *gag* reading frame to abolish export inhibitory sequences) markedly alters Gag assembly competency in select cell types (66, 67, 69).

To begin to decipher links between retroviral gRNA nuclear history and virus particle assembly, we recently used live cell imaging to directly compare the dynamics of HIV-1 gRNA nucleocytoplasmic trafficking in either the Rev/RRE- or CTE-directed nuclear export pathways in single cells over the entire productive phase of infection (81). We found that Rev-dependent gRNAs accumulated in the nucleus prior to "bursting" *en masse* to flood the cytosol in a diffusive pattern. By contrast, replacing the RRE with multiple copies of the CTE derived from the betaretrovirus Mason-Pfizer

monkey virus (MPMV) abolished burst export and linked gRNAs to microtubules for rapid minus end-directed transport to the microtubule organizing center (MTOC). These results demonstrated for the first time that gRNA nuclear export elements program strikingly distinct gRNP trafficking behaviors in the cytoplasm. We have postulated that these differential activities reflect unique requirements of each virus's assembly pathway and efforts are ongoing to discern the unique features of these pathways that could inform the development of novel antiviral strategies.

In this study, we tested a series of competing hypotheses regarding the importance of HIV-1 gRNA cytoplasmic abundance, gRNA subcellular localization, and gRNA nuclear history in regulating the timing and efficiency of HIV-1 particle assembly. We show that altering gRNA cytoplasmic abundance, in a non-coding context, has little to no effect on Gag assembly competency when provided in *trans*. By contrast, perturbing the cytoplasmic localization of gRNAs competent for Gag synthesis can potently reduce the efficiency of HIV-1 virus particle release, despite having only minor effects on cell-associated levels of Gag. The block was explained by perturbations to Gag trafficking leading to aberrant sites of capsid biogenesis and/or defects to capsid assembly or release. Surprisingly, the effect was specific to Gag derived from Rev/RRE-dependent mRNAs, thus confirming that gRNA nuclear history and cytoplasmic trafficking behaviors are crucial determinants of the assembly pathway.

MATERIALS AND METHODS

Cell culture, plasmids, and stable cell lines. Human HeLa and HEK293T cell lines (obtained from the ATCC) were cultured in DMEM (Sigma-Aldrich, Madison, WI, USA) supplemented with 10% fetal bovine serum, 1% L-glutamine, and 1% penicillin-streptomycin. Full-length parental WT HIV-1 proviral plasmids were derived from the pNL4-3 molecular clone (82) inserted into the pBluescript plasmid backbone and bearing inactivating mutations in *env*, *vpr*, and expressing a Firefly Luciferase reporter from the *nef* reading frame (83). 24 copies of the MS2 bacteriophage RNA stem loop (MSL, a kind gift of Robert Singer, Albert Einstein University, New York, NY, USA) were engineered into the full-length pNL4-3 derived constructs as previously described (51). Rev-independent (RevInd) Gag-fluorescent protein (FP) plasmids were derived from a plasmid encoding partially codon-optimized Gag-GFP (a gift of Marilyn Resh, Memorial Sloan Ketterlng Cancer Center, New York, NY, USA) (63, 84). The FP reading frame was fused to RevInd *gag* cDNAs using overlapping PCR and inserted into pcDNA3.1 using *Nhe*I and *Xho*I cut sites. In all instances, mutants of full-length HIV-1 and RevInd Gag plasmids were generated using overlapping PCR. Subgenomic GagFP-MSL HIV-1 expression plasmids encoded Gag fused to mTagBFP2 (85), ECFP, or mCherry upstream of the MSL cassette and inserted into surrogate, subgenomic HIV-1 gRNA plasmid Gag-Pol-Vif-RRE (86). mTagBFP2 was a gift from Michael Davidson (Addgene plasmid # 55302). All GagFP fusions performed similarly. Plasmids pRev and pSynGP (RevInd Gag/Gag-Pol) have been described (65, 87). MS2-YFP targeting constructs were generated by amplifying cDNAs from pMS2-YFP (also a gift of Rob Singer, Albert

147 Einstein University, New York, NY, USA) (88) using overlapping PCR prior to
148 subcloning into a pcDNA3.1 backbone using *Hind*III and *Xho*I cut sites. MS2-mCherry-
149 NLS was generated by overlapping PCR to replace YFP with mCherry reading frames
150 and subcloned into full-length HIV constructs using *Not*I and *Xho*I cut sites. MS2-YFP
151 targeting constructs included an amino-terminal membrane targeting signal derived from
152 the Src kinase (MGSSKSKPKD) (89), amino-terminal LifeAct actin-targeting domain
153 (MGVADLIKKFESISKEE), and/or a carboxy-terminal nuclear localization signal (NLS;
154 PKKKRKV) derived from SV40 Large T antigen (90). An amino-terminal codon-
155 optimized matrix reading frame was engineered onto the MS2-YFP construct to yield
156 MA-MS2-YFP. HeLa.MS2-YFP, HeLa.Gag-CFP, and HEK293T.Gag-CFP stable cell
157 lines were generated as previously described (75, 81). Briefly, desired reading frames
158 were subcloned into a retroviral vector upstream of an internal ribosomal entry site
159 (IRES) and second reading frame encoding Puromycin-N-acetyltransferase (91). High
160 performance clones were selected following limiting dilution in 2µg/mL puromycin.
161
162 **Retroviral assembly assays.** Cells at 30-40% confluency were transfected with 2µg
163 DNA in six well dishes using polyethylenimine (PEI; #23966, Polysciences Inc,
164 Warrington, PA, USA). pcDNA3.1 or pBlueScript were used as empty vector controls.
165 Culture media were replaced at 24 hours post-transfection and cell lysates and
166 supernatants were harvested for immunoblot analysis at 48 hours (69). Briefly, 1mL of
167 harvested culture supernatant was underlaid with 20% sucrose (w/v) in PBS, subjected
168 to centrifugation at >21,000g for two hours at 4ºC, and viral pellets were resuspended in
169 35µL dissociation buffer. Cells were harvested in 500µL radioimmunoprecipitation assay

(RIPA) buffer, lysed by passage through 26G needle, subjected to centrifugation at 1,500g for 20 minutes, and combined 1:1 with dissociation buffer. Proteins were resolved by sodium dodecyl sulfate-polyacrylamide gel electrophoresis (SDS-PAGE) and transferred to nitrocellulose membranes. Gag was detected using a mouse monoclonal antibody recognizing HIV-1 capsid/p24 (183-H12-5C; 1:1000 dilution) from Dr. Bruce Chesebro and obtained from the NIH AIDS Research and Reference Reagent Program (Bethesda, MD, USA) (92) and anti-mouse secondary antibodies conjugated to an infrared fluorophore (IRDye680LT, 1:10000 dilution, Li-Cor Biosciences, Lincoln, NE, USA) for quantitative immunoblotting. As a loading control, heat shock protein 90A/B (HSP90) was detected using a rabbit polyclonal antibody (H-114, 1:2500 dilution, Santa Cruz Biotechnology, Santa Cruz, CA, USA) and anti-rabbit secondary antibodies conjugated to an infrared fluorophore (IRDye800CW, 1:7500 dilution, Li-Cor Biosciences). Fluorescent proteins (CFP, YFP, etc.) were detected using a rabbit polyclonal antibody against full-length GFP (FL, 1:1000 dilution, Santa Cruz Biotechnology) and anti-rabbit secondary antibody conjugated to an infrared fluorophore (IRDye800CW). Where indicated, the protease inhibitor saquinavir (NIH AIDS Research and Reference Reagent program, Bethesda, MD) was added to 5μM at 24 hours post-transfection. Typically, retroviral assembly assays were performed with transfections and harvesting occurring in one week while processing and immunoblotting occurred in the following week. Most results were obtained from three biological replicates as defined as cells plated in six well dishes transfected on separate days (i.e. replicate 1 was transfected on a separate day from replicate 2).

193 **Microscopy and single molecule fluorescence in situ hybridization (smFISH)**.
194 Cells were plated in 24-well glass-bottom dishes (Mattek Corporation, Ashland, MA,
195 USA) or 8-well microslides (IBIDI, Madison, WI, USA) and transfected using PEI.
196 Transfection mixes contained 1µg (24-well) or 333ng (IBIDI) plasmid DNA. De-
197 convolution fixed-cell imaging experiments were performed on a Nikon Ti-Eclipse
198 inverted wide-field microscope (Nikon Corporation, Melville, NY, USA) using a 100x
199 Plan Apo oil objective lens (numerical aperture NA 1.45). These cells were fixed 24-36
200 hours post-transfection in 4% paraformaldehyde in PBS. Live cell imaging experiments
201 were also performed on a Nikon Ti-Eclipse inverted wide-field microscope using a 20x
202 Plan Apo objective lens (NA 0.75) with images acquired every 60 minutes for more than
203 24 hours. Images were acquired using an ORCA-Flash4.0 CMOS camera (Hamamatsu
204 Photonics, Skokie, IL, USA) and using the following excitation/emission filter sets
205 (nanometer ranges): 430/470 (CFP), 510/535 (YFP), 585/610 (mCherry). For fixed cell
206 experiments using smFISH to visualize HIV-1 gRNA, cells were plated and transfected
207 as above. At ~30 hours post-transfection, cells were washed, fixed in 4% formaldehyde,
208 and permeabilized in 70% ethanol for at least four hours at 4ºC. FISH was performed as
209 previously described (88, 93, 94). Custom Stellaris FISH probes were designed to
210 recognize NL4-3 HIV-1 *gag-pol* reading frame nucleotides 386-4614 by utilizing Stellaris
211 RNA FISH Probe Designer (Biosearch Technologies, Inc., Petaluma, CA, USA)
212 available online at www.biosearchtech.com/stellarisdesigner (version 4.1). The samples
213 were hybridized with the Gag/GagPol Stellaris RNA Fish Probe set (48 probes) labeled
214 with CAL Fluor Red 610 dye (Biosearch Technologies, Inc.), following manufacturer's
215 instructions available online at www.biosearchtech.com/stellarisprotocols. Structured

illumination microscopy (SIM) was performed on a Nikon N-SIM microscope using a 100x TIRF oil objective lens (NA 1.49). Images were acquired using an Andor iXon Ultra 897 EMCCD (Andor Technology, Belfast, United Kingdom) and Nikon NIS Elements in 3D-SIM mode using the following excitation laser wavelengths (nanometer ranges): 408 (mTagBFP2), 488 (YFP), and 561 (CAL Fluor Red 610). Widefield epifluorescent microscopy images were deconvolved using NIS Elements. All images were processed and analyzed using FIJI/ImageJ2 (95). Results were obtained from three biological replicates as defined as cells plated in IBIDI slides or 24-well dishes transfected on separate days (i.e. replicate 1 was transfected on a separate day from replicate 2).

Thin section electron microscopy. HEK293T cells were cultured in six-well dishes and transfected as described above. At 48 hours post-transfection, cells were fixed in a solution of 2.5% glutaraldehyde, 2.0% paraformaldehyde in 0.1M sodium phosphate buffer (PBS), pH 7.4 for ~2 hours at room temperature. Samples were rinsed five times for five minutes each in 0.1M PBS. Rinsed cells were post-fixed in 1% osmium tetroxide, 1% potassium ferrocyanide in PBS for 1 hour at room temperature. Following osmium tetroxide post-fixation, the samples were rinsed in PBS, as before, and rinsed three times in distilled water for five minutes to clear phosphates and embedded using increasing concentrations (10mL A/M, 10mL B, 300µL C, 100µL D components) of Durcupan ACM resin (Fluka AG, Switzerland) at 60ºC. Cells were pelleted and sectioned using a Leica EM UC6 ultramicrotome with 100nm sections collected on 300 mesh copper thin-bar grids, and contrasted with Reynolds lead citrate and 8% uranyl

239 acetate in 50% ethanol. Sections were observed with a Phillips CM120 transmission
240 electron microscope, and images were collected with a MegaView III (Olympus-SIS,
241 Lakewood, CO, USA) side-mounted digital camera. All images were processed and
242 analyzed using FIJI/ImageJ2 (95).
243
244 **RESULTS**
245
246 **Tracking Gag/gRNA interactions in single living cells.** To study Gag/gRNA
247 interactions both functionally and using fluorescence microscopy, we inserted 24 copies
248 of the MS2 bacteriophage RNA stem-loop (MS2 stem loops; MSL) recognized by the
249 MS2 coat protein into the major intron and between the *gag* and *pol* open reading
250 frames of a full-length HIV-1 NL4-3-based luciferase reporter virus construct (WT-MSL)
251 (1, 82) (Figure 1). WT-MSL expressed full-length Gag and yielded robust production of
252 virus-like particles (VLPs) released into the cell media from both HeLa and 293T cells,
253 albeit in the absence of virion maturation due to abrogation of *gag-pol* expression
254 (Figures 1B, lane 2). To visualize gRNAs in single cells, MSL-bearing gRNAs were
255 monitored in HeLa cells engineered to stably express the MS2-YFP protein fused to a
256 carboxy-terminal nuclear localization signal (NLS) (HeLa.MS2-YFP) (1, 51). In these
257 cells, low levels of the MS2-YFP protein are sequestered in the nucleus until bound to
258 an MSL-containing gRNA and exported to the cytoplasm (Figure 1C, compare dRRE
259 condition to WT or 1ACG) (81).
260 Investigating the role of gRNAs during the process of assembly is confounded by the
261 gRNA's essential role as the *gag/gag-pol* mRNA (47). Therefore, we generated a

gRNA-only construct (1ACG-MSL) bearing a single nucleotide substitution (ATG>ACG) at the initiator methionine codon of Gag (Figure 1A). To control for cytoplasmic activities, we deleted the RRE in 1ACG-MSL, resulting in a gRNA incapable of exiting the nucleus due to the inability of HIV-1 Rev to regulate CRM1-dependent gRNA nucleocytoplasmic trafficking (dRRE-MSL) (Figure 1A). As expected, neither 1ACG nor dRRE transcripts generated full-length Gag proteins (Figure 1B, compare lanes 3 and 4 to lane 2), although 1ACG transcripts were translationally-competent, yielding the synthesis of low levels of a minor Gag isoform (p40) previously shown to result from initiation at *gag* codon methionine-142 (Figure 1B, lane 3) (96, 97). To supply "gRNA-minus" Gag *in trans* we employed Gag-fluorescent protein (FP = cyan fluorescent protein, mTagBFP2, mCherry, *etc.,* depending on the experiment but shown in blue for consistency) fusion proteins expressed from constructs wherein the *gag* coding region was sufficiently codon-optimized to achieve protein synthesis in the absence of Rev or any other viral factors (RevInd GagFP) (63, 84) (Figures 1A and 1B, lane 5).

Several RNA viruses utilize their genomes as scaffolds to nucleate virion assembly events in the cytoplasm (98–101). Whether HIV-1's gRNA plays a role in the assembly pathway is unclear, thus we first tested if RevInd GagFP trafficking or assembly efficiency was affected by the provision of cytoplasmic HIV-1 gRNAs in *trans*. As expected, expression of WT-MSL and 1ACG-MSL gRNAs yielded translocation of MS2-YFP from the nucleus to the cytoplasm in >50% of transfected HeLa.MS2-YFP cells at ~24 hours post-transfection (Figures 1C and 1D). By contrast, dRRE-MSL gRNAs formed discrete MS2-YFP punctae that were retained in the nucleus in >90% of transfected cells, consistent with gRNA transcription events in the absence of nuclear

export (Figures 1C and 1D). When co-expressed, WT- or 1ACG-gRNAs co-localized with RevInd GagFP aggregates at the plasma membrane, suggesting Gag/gRNA co-trafficking to assembly sites (Figure 1C, bottom panels). However, for each of these conditions, we observed only minor differences to the frequency of cells exhibiting PM-adjacent RevInd GagFP aggregates (Figure 1C, middle panels, and quantification in 1E). Moreover, RevInd GagFP assembled with similar efficiency when co-expressed with either 1ACG- or dRRE-gRNAs in a VLP assembly assay in HEK293T cells (Figure 1F). Thus, RevInd GagFP trafficking is largely unaffected by gRNAs co-expressed in the cytoplasm and accessed in *trans.*

HIV-1 gRNA cytoplasmic abundance plays a minor role in GagFP trafficking at the sub-cooperative threshold. In a second set of experiments, we tested the hypothesis that gRNA cytoplasmic abundance is more relevant to the assembly pathway at low, sub-cooperative levels of Gag expression (Figure 2). To avoid the variability of single cell GagFP expression levels observed due to transfection as for the experiments in Figure 1, we generated HeLa cells that stably expressed low levels of RevInd Gag-CFP (HeLa.Gag-CFP cells) and selected a high performance clone wherein RevInd Gag-CFP was diffuse throughout the cytoplasm but then markedly accumulated in large punctae at the cell surface in response to HIV-1 infection at 24-36 hours post-infection (Figure 2A and Video 1).

Because these cells lacked MS2-YFP, we tracked Gag-CFP in the presence of WT-MSL, 1ACG-MSL, and dRRE-MSL gRNAs modified to express MS2-mCherry-NLS from the native viral promoter (inserted into the *nef* reading frame, Figure 2B). In

HeLa.Gag-CFP cells stably expressing WT-MSL/MS2-mCherry-NLS gRNAs, we observed marked transitions of RevInd Gag-CFP to discrete punctae at the PM of >75% of cells, similar to infection (Figures 2C, left panels and quantification in 2D). The gRNA's MS2-mCherry-NLS signal (yellow) co-localized with surface Gag-CFP (cyan) consistent with Gag/gRNA co-trafficking to the PM and gRNA encapsidation (Figure 2C, lower left panel). Gag-CFP was also released from cells as VLPs under this condition (Figure 2F, compare lane 2 to lane 1). Contrary to our hypothesis, the expression of 1ACG-MSL gRNAs did not drive RevInd Gag-CFP to the PM. Instead, we observed RevInd Gag-CFP as well as cytoplasmic MS2-mCherry-NLS signals coalescing into large cytoplasmic granules in >50% of cells (Figures 2C, middle panels, quantification in 2E, and Video 2). dRRE-MSL expression had no effect on RevInd Gag-CFP distribution, as expected (Figures 2C, right panels, 2D, and 2E). Taken together, these data indicated that a sub-cooperative threshold for Rev-independent Gag assembly cannot be lowered by an excess abundance of cytoplasmic gRNA in single cells, at least when provided in *trans*. In fact, the tendency of 1ACG-gRNAs to aggregate Gag-CFP in large cytoplasmic granules suggests that disproportionately high levels of gRNA in the cytoplasm may actually be detrimental to Gag trafficking.

Perturbing HIV-1 gRNA subcellular localization potently blocks virus particle production. The above experiments indicated that altering gRNA cytoplasmic abundance had little to no effect on Gag subcellular trafficking or assembly competency when provided in *trans.* Thus, we next tested if gRNA subcellular localization is a determinant of the assembly pathway. To this end, we modified MS2-YFP fusion

proteins to carry subcellular trafficking motifs with the goal of artificially targeting MSL-bearing gRNAs to specific cellular membranes or the cytoskeleton (Figures 3-6). We first tested a protein myristoylation signal (MGSSKSKPKD) derived from the proto-oncogene Src kinase, and generated versions of Src-MS2-YFP that would or would not accumulate preferentially in association with the nucleus due to the presence or absence of a carboxy-terminal NLS (Src-MS2-YFP and Src-MS2-YFP-NLS) (Figure 3A). The Src targeting motif was chosen for these experiments because, similar to Gag's MA domain, it targets proteins to PI(4,5)P_2 phospholipid moieties at the cytoplasmic face of the PM (89). Indeed, prior work showed that the assembly of Gag mutants lacking MA is rescued by the addition of an amino-terminal Src membrane targeting motif (15, 54). As a control, we employed a previously validated MS2-NXF1 fusion protein that alters gRNA nucleocytoplasmic transport by biasing it toward the NXF1/NXT1 nuclear export pathway, in competition with Rev and CRM1 (102, 103). Fluorescence microscopy confirmed Src-MS2-YFP at the PM in HeLa cells and Src-MS2-YFP-NLS at the nuclear membrane (Figure 3B).

We hypothesized that Src-MS2-YFP proteins would enhance MSL-dependent gRNA trafficking to the PM, and thus stimulate virus particle assembly. However, we observed the opposite outcome, with co-expression of Src-MS2-YFP or Src-MS2-YFP-NLS causing a greater than ten-fold reduction in VLP release efficiency for Gag derived from our WT-MSL gRNA construct (Figure 3C, compare lanes 3 and 4 to lanes 1 and 2). Both parental WT gRNAs and RevInd GagFP constructs lacking the MSL cassette were largely immune to the MS2 targeting proteins (Figures 3D and 3E), confirming that the effect was specific to MSL-bearing transcripts. Interestingly, the MS2-NXF1 control also

affected VLP release efficiency from the WT-MSL construct. However, this effect was associated with a marked increase to cell-associated Gag, likely reflecting enhanced gRNA nuclear export and/or Gag synthesis through linkage to the NXF1/NXT1 pathway (Figure 3C, lane 5).

Src-MS2-YFP proteins induce a gRNA-specific block to Gag trafficking in *cis*. To explore the mechanism underpinning the Src-MS2-YFP-linked assembly block, we first tracked GagFP molecules expressed from previously validated Rev-dependent GagFP-MSL-RRE surrogate gRNA plasmids (Figure 4A) (81) in the presence or absence of Src-MS2-YFP targeting proteins. Similar to WT-MSL gRNAs, GagFP VLP release was almost completely inhibited by Src-MS2-YFP or Src-MS2-YFP-NLS expression (Figure 4B, compare lanes 3 and 4 to 1 and 2). Moreover, GagFP was less frequently detected at PM punctae under these conditions, consistent with a defect to either Gag intracellular trafficking or Gag cytoplasmic abundance (Figure 4C and quantification in 4D). To distinguish between these two possible explanations, we transfected HEK293T cells with Rev and decreasing amounts of GagFP-MSL-RRE, or a constant amount of Rev and GagFP-MSL-RRE plus increasing amounts of the Src-MS2-YFP construct (Figure 4E). Increasing levels of Src-MS2-YFP lowered the amount of GagFP in VLPs without notable changes to the levels of cell-associated GagFP, a result most consistent with a block to virus particle assembly or release from the cell. We also tested if Src-MS2-YFP proteins could inhibit VLP production in *trans* by co-transfecting RevInd GagFP with 1ACG genomes either lacking or bearing the MSL cassette, and also in the presence or absence of either control MS2-YFP-NLS or inhibitory Src-MS2-YFP

proteins. Src-MS2-YFP did not inhibit assembly by RevInd GagFP under these conditions (Figure 4F, compare lanes 3 and 6 to the controls in lanes 7 and 8), thus confirming that the Src-MS2-YFP-induced, gRNA-dependent assembly inhibition occurs only in *cis*.

Re-targeting gRNAs competent for Gag synthesis to non-PM membranes or F-actin markedly affects Gag trafficking and assembly competency. Because the MS2-YFP proteins were proxies for MSL-bearing RNAs, we confirmed the subcellular localization of native gRNAs using single molecule fluorescence *in situ* hybridization (smFISH) in conjunction with superresolution structured illumination microscopy (SIM). In these experiments, we transfected HeLa cells with Rev-dependent GagFP-MSL-RRE and MS2-YFP fusion proteins with or without Rev, fixed cells at ~30 hours post-transfection, and performed smFISH using a *gag/gag-pol*-specific DNA probe set (Figure 5A). HeLa cells transfected with MS2-YFP-NLS and GagFP-MSL-RRE in the absence of Rev exhibited marked co-localization between MS2-YFP-NLS and the gRNA FISH signal in the nucleus, with no apparent GagFP expression, as expected (Figure 5A, NLS no Rev condition, and Video 3). When Rev was co-expressed, both the MS2-YFP-NLS and gRNA FISH signals were now readily detected in the cytoplasm as well as co-localizing with GagFP at PM-adjacent punctae, (Figure 5A, NLS+Rev condition, and Video 4). These experiments confirmed that the MS2-YFP signals tracked in Figures 1-4 were indeed representative of actual gRNA trafficking and that our system was Rev-responsive.

As expected, Src-MS2-YFP also co-localized with the gRNA smFISH signal, although for this condition Src-MS2-YFP clearly triggered a massive relocalization of gRNAs from a diffuse cytoplasmic distribution to intracellular membranes including, unexpectedly, the nuclear envelope (Figure 5A, Src+Rev condition, and Video 5). Remarkably, we also observed notable accumulations of GagFP at or near these intracellular sites, suggesting VLP assembly and/or aberrant Gag aggregation at non-native subcellular locations (Figure 5A, compare blue panels for NLS+Rev and Src+Rev conditions). Consistent with this hypothesis, thin section electron microscopy on HEK293T cells transfected similarly to express the same MS2-YFP targeting proteins with WT-MSL gRNAs revealed a high frequency of intracellular VLP assembly events for the Src-MS2-YFP condition (Figure 5B and quantification in 5C). Thus, gRNA-directed Gag mistargeting was likely to explain the bulk of the virus particle release defect described in Figures 3 and 4.

Because cortical actin has also been implicated in HIV-1 trafficking/assembly (104–111), we also tested the effects of targeting gRNAs to actin by fusing MS2-YFP to the Lifeact peptide that binds to F-actin bundles (112). Interestingly, Lifeact-MS2-YFP also reduced virus particle production specifically from MSL-bearing gRNAs but to a lesser extent than did the Src-MS2-YFP construct (Figure 5D, compare lanes 5 and 6 to 1 through 4). Both gRNAs and GagFP were observed to co-aggregate with Lifeact-MS2-YFP at or near actin filaments (Figure 5A, Lifeact+Rev condition, and Video 6) and electron micrographs revealed an increase to partial or incomplete VLP budding events (Figure 5B and quantification in 5C).

421 Finally, we tested the effects of an HIV-1 MA-MS2-YFP targeting protein fusing a
422 codon optimized HIV-1 MA domain to the amino-terminus of MS2-YFP. We
423 hypothesized that this configuration would drive MSL-gRNAs to accumulate at virally
424 "appropriate" PM assembly sites (Figure 6A). However, similar to both the Src- and
425 Lifeact-MS2-YFP conditions, MA-MS2-YFP had a potent inhibitory effect on assembly
426 (Figure 6B). GagFP in this condition was successfully trafficked to the PM but was
427 frequently observed forming striking, "worm-like" extensions at the cell surface (Figure
428 6C and Video 7). These data confirmed that re-directing gRNAs to specific subcellular
429 localizations also markedly affects Gag trafficking and can even negatively impact the
430 integrity of the assembly event.
431
432 **The gRNA-linked assembly arrest is specific to Gag derived from Rev/RRE-**
433 **dependent mRNAs.** A remaining conundrum for this study was the fact that Gag is
434 sufficient to drive virus particle assembly at the PM even in the absence of gRNA
435 binding (13, 54, 18). Thus, how can the gRNA be affecting Gag trafficking? One
436 possible explanation for our observations was that, under native conditions, a
437 determinant of the assembly pathway is localized Gag/Gag-Pol translation at the site of
438 gRNA tethering. Should this hypothesis be correct, both native, Rev-dependent gRNAs
439 and our synthetic RevInd GagFP transcripts modified to carry an MSL cassette (Figure
440 7A) should be similarly affected by MS2-based RNA tethering. Contrary to this
441 hypothesis, both Src-MS2-YFP and Lifeact-MS2-YFP actually enhanced VLP
442 production from RevInd Gag-CFP-MSL transcripts (compare Figure 7C to 7B). We also
443 observed that Src-MS-YFP had little to no negative effect on Gag derived from intron-

retaining gRNA constructs rendered Rev-independent by replacing the RRE with four copies of the constitutive transport element (4xCTE) derived from the betaretrovirus Mason-Pfizer monkey virus (Figure 7D). This transcript is exported to the cytoplasm by NXF1/NXT1 instead of CRM1 (76, 87). These results thus implicated the RRE and/or Rev as core determinants of the native Gag/gRNA assembly pathway. Indeed, RevInd Gag-CFP-MSL constructs modified to also carry the RRE became sensitive to Src-MS2-YFP co-expression, but only when co-expressed with Rev (Figure 7E).

Trans-dominant Gag mutants specifically reduce the assembly of Gag derived from Rev/RRE-dependent transcripts. The above experiments revealed an unexpected link between gRNA nuclear history (*i.e.,* nuclear export via the RRE/Rev/CRM1 pathway), gRNA distribution in the cytoplasm, and Gag assembly competency. Because spatial perturbations of gRNA trafficking could represent a yet untapped antiviral strategy, we tested the effects of disrupting native HIV-1 gRNAs not bearing the MSL cassette by overexpressing Gag proteins competent for gRNA binding (due to an intact NC domain) but mutated to no longer traffic to the PM (Figure 8). To this end, we co-transfected HEK293T cells to express either Rev-independent synthetic Gag/Gag-Pol transcripts (RevInd Gag-Pol) or the full-length, parental WT HIV gRNA in the presence or absence of each of the following versions of RevInd Gag-CFP: assembly competent RevInd Gag-CFP (84), non-myristoylated RevInd Gag-G2A-CFP (113), MA-deficient RevInd Gag-p40-CFP (96), and NC deficient RevInd Gag-dNCzip-CFP (15). None of these RevInd Gag-CFP mutants notably affected expression and assembly of Gag derived from the RevInd Gag-Pol construct (Figure 8A). However, VLP

assembly for Gag derived from the parental WT construct was reduced for all of the assembly-defective conditions, provided that the *trans*-acting Gag protein encoded an intact NC domain (Figure 8B, compare lanes 4-5 to lane 6). The inhibitory assembly effects were limited to Gag encoded from a WT gRNA (and not the synthetic, RevInd Gag/Gag-Pol) and were not observed when WT HIV was co-transfected with RevInd dNCzip-CFP. Assembly inhibition was native gRNA-dependent and likely to involve disruption of *cis* interactions between gRNA and its protein product, Gag. Thus, there appear to be strong links between gRNA nuclear history and the susceptibility of Gag to *trans*-acting inhibitory elements.

DISCUSSION

For retroviruses, gRNA nucleocytoplasmic transport is a highly ordered process ensuring robust late gene expression and efficient genome encapsidation during virion assembly. Herein we provide, to our knowledge, the first direct evidence that gRNA subcellular distribution represents a core determinant of HIV-1's assembly pathway. Altering the cytoplasmic abundance of non-coding, 1ACG-gRNAs had little to no effect on Gag-FP trafficking or assembly in a *trans* context (Figures 1 and 2). By contrast, artificially tethering gRNAs to cellular membranes or the actin cytoskeleton markedly affected Gag trafficking in *cis* and potently reduced virus particle release (Figures 3 through 6). MS2-retargeted gRNAs (detected by FISH) and Gag coalesced together at aberrant sites within the cell thus indicating that gRNAs encode one or more signaling activities relevant to the assembly pathway. Unexpectedly, we mapped this signal to the

Rev/RRE nuclear export module that regulates CRM1-dependent gRNA nuclear export (Figure 7). That Gag derived from Rev-independent mRNAs was largely immune to the effects of RNA tethering (Figures 7C and 7D) or *trans*-dominant Gag proteins (Figure 8) supports a model wherein specialized links between HIV-1 Rev function and gRNA cytoplasmic trafficking regulate Gag's assembly potential (Figure 9).

We initially hypothesized that increasing the net abundance of PM-proximal gRNAs would stimulate virus particle assembly should gRNAs encode one or more signals relevant to the nucleation of the assembly event. However, overexpressing "Gag-minus" 1ACG-gRNAs in *trans* had little to no effect on assembly either at high (Figure 1) or low (Figure 2) levels of GagFP. In fact, 1ACG-gRNAs arrested GagFP in cytoplasmic granules in our stable "low" GagFP cell line, suggesting that suboptimal Gag-gRNA stoichiometry is detrimental to the formation and transit of gRNP trafficking complexes. Efforts to bias gRNP trafficking to the PM using our MS2-based RNA tethering strategy were also not beneficial to assembly, but instead potently inhibited particle production for Gag derived from gRNAs or Rev-dependent *gag-pol* mRNAs (Figures 3-7). Based on these observations we reason that, under native conditions, HIV-1 must maintain a careful balance of Gag-gRNA interactions (and likely interactions with host factors) that prevent gRNP aggregation or accumulation in subcellular locations other than preferred sites of assembly (i.e., the "bad neighborhood" model, see Figure 9).

Single-molecule FISH coupled to superresolution microscopy in HeLa cells confirmed that Src-MS2-YFP proteins markedly altered MSL-gRNA distribution away from a "typical" diffusive pattern in the cytosol to accumulate preferentially at

membranes (Figure 5A). However, we were surprised to observe that gRNAs and Gag did not accumulate at the PM under these conditions, but instead co-localized at or near the nuclear membrane or in association with vesicles distributed throughout the cytoplasm. This aberrant distribution and observations of intracellular assembly events (Figure 5B) likely explain the profound block to VLP release. Lifeact-MS2-YFP and MA-MS2-YFP also markedly reduced the efficiency of virus particle production in the context of MSL-gRNAs but apparently through alternative mechanisms (Figures 5 and 6). Lifeact-MS2-YFP caused a re-distribution of gRNAs and Gag into linear arrays defined by F-actin filaments at or near the PM (Figure 5A and Video 6), with an increase to the occurrence of partially budded particles (Figures 5B and 5C) reminiscent of a late budding defect (32, 114). MA-MS2-YFP's effects were more dramatic, causing GagFP to form striking, worm-like aggregates at the PM (Figure 6) resembling previously reported defects to the formation of the immature capsid lattice (115–119). In sum, these results demonstrate unambiguously that physically perturbing HIV-1 gRNA cytoplasmic trafficking can have profound effects on the assembly pathway independent of effects on Gag synthesis. Moreover, we it is intriguing that each MS2 targeting protein affected a distinct phase of pathway; site of assembly (S-MS2-YFP), late stage budding (Lifeact-MS2-YFP), or capsid assembly (MA-MS2-YFP).

Regarding the mechanistic link between gRNA subcellular distribution and the assembly pathway, we found that S-MS2-YFP's inhibitory activity (and to a lesser extent, that of Lifeact-MS2-YFP) was specific to gRNAs and surrogate *gag/gag-pol* mRNAs encoding the RRE and expressed in the presence of Rev (Figure 7). Thus, Gag's vulnerability to this mode of inhibition is tied to gRNA nuclear history. We cannot

yet fully explain the molecular basis for Rev/RRE specificity. Several genetic studies indicate that Rev-dependent and Rev-independent mRNAs are differentially regulated in the cytoplasm (35, 81, 87, 120–126). Moreover, we and others have previously shown that gRNA nuclear history can affect Gag subcellular trafficking and/or assembly efficiency (47, 69, 75, 87, 127–129). In this context, we recently showed using live cell imaging that HIV-1 gRNAs or heterologous mRNAs modified to bear the RRE and expressed in the presence of Rev exhibit unique, CRM1-driven "burst" nuclear export events wherein transcripts flood the cytoplasm *en masse* and prior to the onset of protein synthesis, thus yielding the diffusive distribution gRNAs in the cytoplasm shown in Figure 1C (81). Thus, unique spatiotemporal features of the Rev-regulated burst (*e.g.,* punctuated, rapid increases to free Gag/gRNP abundance in the cytoplasm, or diffusion in itself) likely influence core aspects of the assembly pathway.

Indeed, large gRNP complexes trafficking through the cytoplasm prior to utilization draw parallels with cellular mRNA molecules that are translated locally (2–4). We suggest that perturbations to the ability of gRNAs to freely diffuse through a dense cytoplasmic fluid may have negative consequences for localized translation and subsequent virion assembly. The nuclear coating/coding of gRNAs with cellular factors may also influence the size, hydrophobicity, and fluid phase of HIV-1 gRNP complexes. Several host post-transcriptional regulatory factors are implicated in the regulation of HIV-1 gRNA trafficking and/or translation (47–49, 130). One or more co-factors tied to the Rev/RRE/CRM1 transport module may represent a "missing link" between Rev function and Gag assembly competency. In this context, it is worth noting that Kutluay *et*

558 *al.* recently provided evidence from CLIP-seq analysis for a direct interaction between
559 Gag and the RRE of as yet unknown functional relevance (39).

560 Finally, it remains a conundrum that Gag derived from Rev-independent mRNAs
561 (e.g., RevInd GagFP or Gag derived from 4xCTE-dependent mRNAs) is largely
562 resistant to MS2-tethering or trans-dominant Gag proteins. However, this dichotomy
563 emphasizes specific vulnerabilities to the Rev/RRE pathway that may be relevant to the
564 development of novel anti-HIV strategies. To date, there are no FDA-approved antiviral
565 approaches that perturb HIV-1 gene expression or the stages upstream of immature
566 virus particle assembly, although several strategies have been pursued including
567 disruption of Tat or Rev function, virus-specific miRNAs, and trans-dominant proteins
568 [reviewed in (131)]. Our results suggest that strategies to successfully disrupt viral
569 mRNA subcellular distribution or fluid phase transitions using small molecule inhibitors
570 or alternative strategies (*e.g.*, provision of *trans*-acting synthetic “restriction” factors via
571 gene therapy) merit further exploration.

572

573 **ACKNOWLEDGEMENTS**

574 This study was supported by funding from the National Institutes for Health / National
575 Institute of Allergy and Infectious Diseases (RO1AI110221A1) and the Greater
576 Milwaukee Foundation’s Shaw Scientist Program to N.M.S.. J.T.B. is a trainee of the
577 National Science Foundation Graduate Research Fellow Program (grant DGE-
578 1256259). Any opinions, findings, and conclusions or recommendations expressed in
579 this material are those of the authors and do not necessarily reflect the views of the
580 National Science Foundation. We gratefully acknowledge Randall Massey and the

581 University of Wisconsin SMPH Electron Microscopy Facility for assistance with
582 processing and imaging EM. We gratefully acknowledge Elle Kielar Grevstad and the
583 University of Wisconsin Biochemistry Optical Core for assistance with structured
584 illumination microscopy. The following reagents were obtained through the NIH AIDS
585 Reagent Program, Division of AIDS, NIAID, NIH: HIV-1 p24 Hybridoma (183-H12-5C)
586 (from Dr. Bruce Chesebro) and Saquinavir.
587

FIGURE LEGENDS

Figure 1. Tracking Gag/gRNA interactions in single living cells. (A) Cartoon depiction of gRNAs used in these studies. Ψ = Psi packaging signal. MSL = 24 copies of MS2 RNA stem loop. RRE = Rev-response element. *Tat* and *rev* are gene-regulatory elements made from multiply-spliced mRNAs. *Vif* and *vpu* are immune modulatory genes made from singly-spliced mRNAs. (B) HEK293T cells were transfected with 2000ng HIV-1 plasmids encoding gRNAs depicted in A. VLPs and cell lysates were collected 48 hours post-transfection, resolved by SDS-PAGE, and immunoblotted for Gag and HSP90 as a loading control. (C) Widefield deconvolution microscopy images of HeLa.MS2-YFP cells transfected with 100ng RevInd GagFP and 900ng HIV constructs, fixed ~30 hours post-transfection, and imaged. Single Z-plane images are shown. Scale bars represent 10 microns in full images, 2 microns in regions of interest (ROI). Dashed white lines show the relative position of cell nuclei. White box outlines the ROI. Red arrows indicate sites where RevInd GagFP has accumulated in PM-adjacent punctae. (D) Quantification of MS2-YFP localization phenotypes. Bar graphs show percent of cells with nuclear, cytoplasmic, or both distributions of gRNA for each transfection condition. (E) Quantification of GagFP distribution phenotypes. Bar graphs show percent of cells with diffuse or PM-adjacent punctae Gag localization in each transfection condition. (D & E) Error bars represent standard deviation from the mean for at least four independent experiments quantifying at least 100 cells per condition. (F) HEK293T cells were co-transfected with 500ng RevInd GagFP and 1500ng of HIV gRNA constructs as indicated or an empty vector control (pBluescript) and immunoblotted as in 1A. Bar graphs show fold change in Gag release factor relative to

611 empty vector condition. Release factor is calculated by Gag band intensities in VLPs
612 divided by lysates normalized to HSP90 (N=4).
613
614 **Figure 2. HIV-1 gRNA cytoplasmic abundance plays a minor role in GagFP**
615 **trafficking at the sub-cooperative threshold.** (A) Widefield deconvolution microscopy
616 images from live cell imaging experiments of HeLa.Gag-CFP cells infected with WT
617 NL4-3 E-R- virions. This virus expresses mCherry as a reporter for successful infection.
618 Multi-channel images were acquired once per hour for up to 48 hours beginning at ~1
619 hours post-infection. Scale bars represent 10 microns. Red arrows indicate sites where
620 stably expressed RevInd Gag-CFP has accumulated in PM-adjacent punctae. (B)
621 Example of WT-MSL gRNA used in experiments below. These gRNAs are identical to
622 those depicted in Figure 1A with the addition of MS2-mCherry-NLS as a reporter and
623 gRNA-tagging protein expressed from the viral *nef* gene position. (C) Widefield
624 deconvolution microscopy images of stable HeLa.Gag-CFP cells transfected with
625 1000ng HIV gRNA constructs, fixed ~30 hours post-transfection, and imaged. Scale
626 bars represent 10 microns in full images, 2 microns in ROI. Dashed white lines show the
627 relative position of cell nuclei. White box outlines the ROI. Red arrows indicate sites
628 where stably expressed Gag has accumulated: in PM-adjacent punctae for WT-MSL
629 and in the cytoplasm for 1ACG-MSL and dRRE-MSL. Dashed red line in ROI represents
630 edge of cell. (D & E) Quantification of Gag-CFP distribution phenotypes from live cell
631 imaging experiments performed similar to Figure 2A. HeLa.Gag-CFP cells were
632 transfected with 333ng of gRNA constructs (WT-MSL, 1ACG-MSL, and dRRE-MSL also
633 encoding MS2-mCherry-NLS as a reporter and gRNA tagging protein). (D) Bar graphs

show percent of cells with diffuse or PM-adjacent punctae Gag localization. (E) Bar graph shows percent of cells with diffuse, granules, or PM-adjacent punctae Gag localization. (D & E) Error bars represent standard deviation from the mean. At least 30 cells were quantified per transfection condition per experiment (N=3). (F) HEK293T.Gag-CFP cells were transfected with 2000ng of HIV gRNA constructs as indicated or an empty vector control (pBluescript) and immunoblotted for Gag and HSP90. Bar graphs show fold change in Gag release factor relative to empty vector condition (N=3). The asterisk (*) indicates stable GagFP release factor for WT-MSL condition is significantly different from empty vector condition (Two-tailed Student's t-test, p=0.0006).

Figure 3. Perturbing HIV-1 gRNA subcellular localization potently blocks virus particle production. (A) Cartoon depiction of MS2-YFP targeting protein constructs used in these studies. Short name used in subsequent figures is underlined. Amino acid targeting motif is shown at their relative (amino- or carboxy-terminal) position. (B) Widefield deconvolution microscopy images of HeLa cells transfected with 333ng MS2-YFP targeting constructs, fixed ~30 hours post-transfection, and imaged. Scale bars represent 10 microns. Dashed white lines show the relative position of cell nuclei. Dashed cyan lines show the edge of cell. (C) HEK293T cells were transfected with 1000ng MS2-YFP targeting constructs as indicated and 1000ng of WT-MSL and immunoblotted for Gag and HSP90. Bar graphs show release factor relative to Free MS2-YFP. Error bars represent standard deviation from the mean of three independent experiments. The asterisks (*) indicate Pr55 Gag release factor is significantly different

for comparisons indicated by black bars (two-tailed Student's t-test, p=0.023 Src & 0.015 Src+NLS). (D) HEK293T cells were transfected with 1000ng MS2-YFP targeting constructs as indicated and 1000ng of WT NL4-3 E-R- and immunoblotted for Gag and HSP90. Cells were treated with the HIV-1 protease inhibitor saquinavir to prevent Pr55 Gag proteolytic processing and aid quantification of Gag expression and release. Bar graphs show release factor relative to Free MS2-YFP. Error bars represent standard deviation from the mean of three independent experiments. No conditions were significantly different. (E) HEK293T cells were transfected with 1000ng MS2-YFP targeting constructs as indicated and 1000ng of RevInd GagFP immunoblotted for Gag and HSP90. Bar graphs show release factor relative to Free MS2-YFP. Error bars represent standard deviation from the mean of three independent experiments.

Figure 4. Src-MS2-YFP proteins induce a gRNA-specific block to Gag trafficking in *cis*. (A) Cartoon depiction of subgenomic HIV-1 GagFP-MSL-RRE construct used. Splice donor (SD) and splice acceptor (SA) are shown to emphasize that the viral *gagfp* mRNA (surrogate gRNA) retains an intron. (B) HEK293T cells were transfected with 1000ng MS2-YFP targeting constructs as indicated, 900ng of GagFP-MSL-RRE, and 100ng pRev and immunoblotted for Gag and HSP90. Bar graphs show release factor relative to Free MS2-YFP. Error bars represent standard deviation from the mean of three independent experiments. The asterisks (*) indicate Pr55 Gag release factor is significantly different for comparisons indicated by black bars (two-tailed Student's t-test, p=0.03). (C) Widefield deconvolution microscopy images of HeLa cells transfected with 100ng MS2-YFP targeting constructs, 800ng subgenomic GagFP-MSL-RRE, and

pRev, fixed ~30 hours post-transfection, and imaged. Scale bars represent 10 microns in full images, in regions of interest (ROI). Dashed white lines show the relative position of cell nuclei. White box outlines the ROI. Red arrows indicate sites where GagFP has accumulated. (D) Quantification of GagFP localization phenotypes. Bar graphs show percent of cells with vesicular, diffuse cytoplasmic, or PM-adjacent/puncate for each transfection condition. Error bars represent standard deviation from the mean for three independent experiments quantifying at least 100 cells per condition. (E) HEK293T were transfected with decreasing amounts of GagFP-MSL-RRE (1500/1000/500ng) plus 200ng Rev and empty vector as filler up to 2µg total DNA in lanes 1-3. Cells were transfected with 1500ng GagFP-MSL-RRE, plus 200ng Rev, empty vector as filler, and increasing amounts (100/200/300ng) of Src-MS2-YFP and immunoblotted for Gag and HSP90. Bar graphs show release factor relative to lane 1. Error bars represent standard deviation from the mean of three independent experiments. (F) HEK293T cells were transfected with 500ng RevInd Gag-CFP, 100ng MS2-YFP targeting construct as indicated, and 1400ng empty vector, 1ACG (no MSL), or 1ACG-MSL in lanes 1-6. Lanes 7-8 were transfected with 1400ng GagFP-MSL-RRE, 100ng MS2-YFP targeting construct as indicated, 200ng Rev, and 300ng empty vector immunoblotted for Gag and HSP90.

Figure 5. Gag accumulates at sites of mislocalized HIV-1 gRNA. (A) HeLa cells were transfected with 800ng GagFP-MSL-RRE, 100ng MS2-YFP targeting constructs as indicated, and 100ng Rev or empty vector as indicated. Cells were fixed at ~30 hours

post-transfection, subjected to FISH staining, and multi-Z stack images acquired by structured-illumination microscopy (SIM) using a 100x (NA 1.49) TIRF oil objective. Single Z-plane images are shown with scale bars representing 5 microns. White arrows indicate points of interest highlighting colocalization. Nucleus = “nuc”, cytoplasm = “cyto”. (B) HEK293T cells were transfected with 1800ng WT-MSL and 200ng MS2-YFP targeting constructs as indicated for EM. Samples were prepared and images were acquired as described in Materials and Methods. Red arrows indicate representative particle events for budding (NLS), intracellular (Src), and incomplete (Lifeact). (C) Quantification of particles with budding phenotypes. Bar graph shows percent of assembly events exhibiting intracellular, incomplete, or budding phenotype. Errors bars represent standard deviation from the mean of 10 cells imaged. At least 100 budding events were quantified per transfection condition. (D) HEK293T cells were transfected with 100ng MS2-YFP targeting constructs as indicated and either 1700ng RevInd GagFP with empty vector OR 1700ng of GagFP-MSL-RRE with 200ng pRev and immunoblotted for Gag and HSP90. Bar graphs show release factor relative to MS2-YFP-NLS condition for each Gag type (RevInd GagFP or GagFP-MSL-RRE). Error bars represent standard deviation from the mean of three independent experiments. The asterisks (*) indicate GagFP release factor is significantly different for comparisons indicated by black bars (two-tailed Student’s t-test, p=0.0001).

Figure 6. Re-directing HIV-1 gRNAs using MA-MS2 negatively impact Gag assembly and release competency. (A) Cartoon depiction of MA-MS2-YFP targeting protein construct. Widefield deconvolution microscopy image of HeLa cell transfected

with 333ng MS2-YFP targeting constructs, fixed ~30 hours post-transfection, and imaged. Scale bar represent 10 microns. The basal surface (adjacent to the coverslip) is shown. (B) HEK293T cells were transfected with 100ng MA-MS2-YFP targeting construct and 1700ng of GagFP-MSL-RRE with 200ng pRev immunoblotted for Gag and HSP90. Numbers show release factor relative to MS2-YFP-NLS condition from a single experiment. (C) Widefield deconvolution microscopy images of HeLa cells transfected with 100ng MA-MS2-YFP, 800ng GagFP-MSL-RRE and 100ng pRev, fixed ~30 hours post-transfection, subjected to smFISH staining, and imaged. Scale bars represent 10 microns in full images, 2 microns in regions of interest (ROI). The basal surface (adjacent to the coverslip) is shown. White box outlines the ROI. White arrows indicate sites where GagFP has accumulated in worm-like tubules.

Figure 7. The gRNA-linked assembly arrest is specific to Gag derived from Rev/RRE-dependent mRNAs. (A) Cartoon depiction of constructs used in these studies. 4xCTE = four copies of the constitutive transport element from Mason-Pfizer monkey virus. (B-D) HEK293T cells were transfected with 100ng MS2-YFP targeting constructs as indicated and 1700ng of GagFP-MSL-RRE and 200ng pRev (B), 1700ng GagFP-MSL-CTE and 200ng empty vector (C), or 1700ng RevInd GagFP-MSL and 200ng empty vector (D). VLPs and cell lysates were immunoblotted for Gag and HSP90. Bar graphs show release factor relative to MS2-YFP-NLS. Error bars represent standard deviation from the mean of three independent experiments. The asterisks (*) indicate GagFP release factor is significantly different for comparisons indicated by black bars (two-tailed Student's t-test, p=0.018 Src & 0.047 Lifeact). (E) HEK293T cells

were transfected with 100ng MS2-YFP targeting constructs as indicated, 1700ng of RevInd GagFP-MSL-RRE, and either 200ng empty vector or pRev and immunoblotted for Gag and HSP90. Bar graphs show release factor relative to Free MS2-YFP. Error bars represent standard deviation from the mean of three independent experiments. The asterisks (*) indicate GagFP release factor is significantly different for comparisons indicated by black bars (two-tailed Student's t-test, p=0.007).

Figure 8. Trans-dominant Gag mutants specifically reduce the assembly of Gag derived from Rev/RRE-dependent transcripts. HEK293T cells were transfected with 1000ng synthetic RevInd Gag/Gag-Pol construct (A) or WT NL4-3 E-R- (B) and 1000ng of empty vector, RevInd GagFP, G2A GagFP, p40 GagFP, or dNCzip GagFP. Cells were treated with the HIV-1 protease inhibitor saquinavir to prevent Pr55 Gag proteolytic processing and aid quantification of Gag expression and release. VLPs and cell lysates were immunoblotted for Gag and HSP90. Bar graphs show Pr55 Gag release factor relative to empty vector. Error bars represent standard deviation from the mean of three independent experiments.

Figure 9. Right place, right time model for HIV-1 gRNA trafficking, Gag translation, and virion assembly. HIV-1 gRNA (red wiggly line) are exported from the nucleus via the RRE/Rev/CRM1 pathway. Once in the cytoplasm, the HIV-1 gRNA are translated (purple ribosomes) to yield some amount of the Gag polyprotein. We suggest that these HIV-1 gRNAs freely diffuse toward the PM where gRNA dimerization, high-order Gag multimerization, and virion assembly occur. If these gRNAs are redirected to different

772 subcellular locales ("Bad Neighborhoods") such as intracellular vesicles (tan circles) or
773 actin filaments (black chalk lines), Gag trafficking is similarly redirected and virion
774 assembly is subsequently inhibited. In our system, using Src-MS2-YFP and Lifeact-
775 MS2-YFP we have observed this redirection and inhibition that occurs via *cis*
776 interactions between Gag and gRNA and is RRE/Rev-dependent. It is possible that
777 gRNAs exported through the CRM1 pathway are marked, restructured, or coated by
778 some as of yet unknown "missing link" indicated here by pink factor X.
779
780 **Video 1. HIV-1 infection induces accumulation of stably-expressed GagFP into**
781 **assembly sites at the PM.** Live cell imaging of HeLa.Gag-CFP (cyan) cells infected
782 with WT NL4-3 E-R- virions expressing an mCherry (red) as a reporter for successful
783 infection. Images were acquired once per hour and are shown here at 4 frames per
784 second. Scale bar represents 10 microns. White arrows indicate sites where stably
785 expressed RevInd Gag-CFP has accumulated in PM-adjacent punctae.
786
787 **Video 2. HIV-1 gRNA induces accumulation of stably-expressed GagFP into**
788 **cytoplasmic granules.** Live cell imaging of HeLa.Gag-CFP (cyan) cells transfected
789 with 1ACG-MSL/MS2-mCherry (yellow). Images were acquired once per hour and are
790 shown here at 4 frames per second. Scale bar represents 10 microns. White arrows
791 indicate sites where stably expressed RevInd Gag-CFP and MS2-mCherry-tagged
792 gRNA have accumulated in cytoplasmic granules.
793

Video 3. Three-dimensional view of MS2-YFP-NLS and smFISH tagged HIV-1 gRNA. SIM image reconstructed in 3D using FIJI/ImageJ2. Scale bar represents 5 microns. MS2-YFP (green) and gRNA FISH (red) are sequestered in the nucleus in the absence of the Rev protein. White arrow indicates edge of nucleus (nuclear envelope).

Video 4. Three-dimensional view of MS2-YFP-NLS, smFISH tagged HIV-1 gRNA, and HIV-1 Gag. SIM image reconstructed in 3D using FIJI/ImageJ2. Scale bar represents 5 microns. MS2-YFP (green) and gRNA FISH (red) colocalize in the cytoplasm and at the PM with Gag (blue). White arrows indicate colocalized MS2-YFP, gRNA, and Gag punctae at PM.

Video 5. Three-dimensional view of Src-MS2-YFP, smFISH tagged HIV-1 gRNA, and HIV-1 Gag. SIM image reconstructed in 3D using FIJI/ImageJ2. Scale bar represents 5 microns. MS2-YFP (green) and gRNA FISH (red) colocalize at intracellular vesicles and the nuclear periphery with Gag (blue). White arrows indicate colocalized MS2-YFP, gRNA, and Gag punctae at intracellular membranes.

Video 6. Three-dimensional view of Lifeact-MS2-YFP, smFISH tagged HIV-1 gRNA, and HIV-1 Gag. SIM image reconstructed in 3D using FIJI/ImageJ2. Scale bar represents 5 microns. MS2-YFP (green) and gRNA FISH (red) colocalize along linear F-actin filaments with Gag (blue). White arrows indicate colocalized MS2-YFP, gRNA, and Gag punctae along actin filaments.

817 **Video 7. MA-MS2-YFP induces formation of worm-like tubules of GagFP at the**
818 **PM.** Live cell imaging of HeLa cells transfected with MA-MS2-YFP and GagFP-MSL-
819 RRE. Only GagFP channel is shown (cyan). Images were acquired once every 30
820 seconds and are shown here at 4 frames per second. Scale bar represents 2 microns.
821 White arrow highlights a worm-like tubule of GagFP.
822

REFERENCES

1. **Bertrand E**, **Chartrand P**, **Schaefer M**, **Shenoy SM**, **Singer RH**, **Long RM**. 1998. Localization of ASH1 mRNA particles in living yeast. Mol Cell **2**:437–445.

2. **Lécuyer E**, **Yoshida H**, **Parthasarathy N**, **Alm C**, **Babak T**, **Cerovina T**, **Hughes TR**, **Tomancak P**, **Krause HM**. 2007. Global analysis of mRNA localization reveals a prominent role in organizing cellular architecture and function. Cell **131**:174–187.

3. **Donnelly CJ**, **Fainzilber M**, **Twiss JL**. 2010. Subcellular communication through RNA transport and localized protein synthesis. Traffic Cph Den **11**:1498–1505.

4. **Sinnamon JR**, **Czaplinski K**. 2011. mRNA trafficking and local translation: the Yin and Yang of regulating mRNA localization in neurons. Acta Biochim Biophys Sin **43**:663–670.

5. **Buxbaum AR**, **Haimovich G**, **Singer RH**. 2015. In the right place at the right time: visualizing and understanding mRNA localization. Nat Rev Mol Cell Biol **16**:95–109.

6. **Jouvenet N**, **Neil SJD**, **Bess C**, **Johnson MC**, **Virgen CA**, **Simon SM**, **Bieniasz PD**. 2006. Plasma membrane is the site of productive HIV-1 particle assembly. PLoS Biol **4**:e435.

7. **Davis NL**, **Rueckert RR**. 1972. Properties of a ribonucleoprotein particle isolated from Nonidet P-40-treated Rous sarcoma virus. J Virol **10**:1010–1020.

844 8. **Briggs JAG**, **Kräusslich H-G**. 2011. The molecular architecture of HIV. J Mol Biol
845 **410**:491–500.

846 9. **Butsch M**, **Boris-Lawrie K**. 2002. Destiny of unspliced retroviral RNA: ribosome
847 and/or virion? J Virol **76**:3089–3094.

848 10. **Johnson SF**, **Telesnitsky A**. 2010. Retroviral RNA dimerization and packaging:
849 the what, how, when, where, and why. PLoS Pathog **6**:e1001007.

850 11. **Jouvenet N**, **Lainé S**, **Pessel-Vivares L**, **Mougel M**. 2011. Cell biology of
851 retroviral RNA packaging. RNA Biol **8**:572–580.

852 12. **Kuzembayeva M**, **Dilley K**, **Sardo L**, **Hu W-S**. 2014. Life of psi: How full-length
853 HIV-1 RNAs become packaged genomes in the viral particles. Virology.

854 13. **Wills JW**, **Craven RC**. 1991. Form, function, and use of retroviral gag proteins.
855 AIDS Lond Engl **5**:639–654.

856 14. **Ono A**, **Demirov D**, **Freed EO**. 2000. Relationship between human
857 immunodeficiency virus type 1 Gag multimerization and membrane binding. J
858 Virol **74**:5142–5150.

859 15. **Accola MA**, **Strack B**, **Göttlinger HG**. 2000. Efficient particle production by
860 minimal Gag constructs which retain the carboxy-terminal domain of human
861 immunodeficiency virus type 1 capsid-p2 and a late assembly domain. J Virol
862 **74**:5395–5402.

16. **Datta SAK**, **Zhao Z**, **Clark PK**, **Tarasov S**, **Alexandratos JN**, **Campbell SJ**, **Kvaratskhelia M**, **Lebowitz J**, **Rein A**. 2007. Interactions between HIV-1 Gag molecules in solution: an inositol phosphate-mediated switch. J Mol Biol **365**:799–811.

17. **Crist RM**, **Datta SAK**, **Stephen AG**, **Soheilian F**, **Mirro J**, **Fisher RJ**, **Nagashima K**, **Rein A**. 2009. Assembly properties of human immunodeficiency virus type 1 Gag-leucine zipper chimeras: implications for retrovirus assembly. J Virol **83**:2216–2225.

18. **Datta SAK**, **Rein A**. 2009. Preparation of recombinant HIV-1 gag protein and assembly of virus-like particles in vitro. Methods Mol Biol Clifton NJ **485**:197–208.

19. **Olety B**, **Ono A**. 2014. Roles played by acidic lipids in HIV-1 Gag membrane binding. Virus Res.

20. **Ono A**, **Freed EO**. 1999. Binding of human immunodeficiency virus type 1 Gag to membrane: role of the matrix amino terminus. J Virol **73**:4136–4144.

21. **Saad JS**, **Miller J**, **Tai J**, **Kim A**, **Ghanam RH**, **Summers MF**. 2006. Structural basis for targeting HIV-1 Gag proteins to the plasma membrane for virus assembly. Proc Natl Acad Sci U S A **103**:11364–11369.

22. **Ghanam RH**, **Samal AB**, **Fernandez TF**, **Saad JS**. 2012. Role of the HIV-1 Matrix Protein in Gag Intracellular Trafficking and Targeting to the Plasma Membrane for Virus Assembly. Front Microbiol **3**:55.

883 23. **Mercredi PY**, **Bucca N**, **Loeliger B**, **Gaines CR**, **Mehta M**, **Bhargava P**,
884 **Tedbury PR**, **Charlier L**, **Floquet N**, **Muriaux D**, **Favard C**, **Sanders CR**, **Freed**
885 **EO**, **Marchant J**, **Summers MF**. 2016. Structural and Molecular Determinants of
886 Membrane Binding by the HIV-1 Matrix Protein. J Mol Biol.

887 24. **Ganser-Pornillos BK**, **Yeager M**, **Sundquist WI**. 2008. The structural biology of
888 HIV assembly. Curr Opin Struct Biol **18**:203–217.

889 25. **Sundquist WI**, **Kräusslich H-G**. 2012. HIV-1 Assembly, Budding, and Maturation.
890 Cold Spring Harb Perspect Med **2**.

891 26. **Berkowitz RD**, **Ohagen A**, **Höglund S**, **Goff SP**. 1995. Retroviral nucleocapsid
892 domains mediate the specific recognition of genomic viral RNAs by chimeric Gag
893 polyproteins during RNA packaging in vivo. J Virol **69**:6445–6456.

894 27. **D'Souza V**, **Summers MF**. 2005. How retroviruses select their genomes. Nat Rev
895 Microbiol **3**:643–655.

896 28. **Muriaux D**, **Darlix J-L**. 2010. Properties and functions of the nucleocapsid protein
897 in virus assembly. RNA Biol **7**:744–753.

898 29. **Keane SC**, **Heng X**, **Lu K**, **Kharytonchyk S**, **Ramakrishnan V**, **Carter G**, **Barton**
899 **S**, **Hosic A**, **Florwick A**, **Santos J**, **Bolden NC**, **McCowin S**, **Case DA**, **Johnson**
900 **BA**, **Salemi M**, **Telesnitsky A**, **Summers MF**. 2015. Structure of the HIV-1 RNA
901 packaging signal. Science **348**:917–921.

902 30. **Borsetti A**, **Ohagen A**, **Göttlinger HG**. 1998. The C-terminal half of the human
903 immunodeficiency virus type 1 Gag precursor is sufficient for efficient particle
904 assembly. J Virol **72**:9313–9317.

905 31. **Martin-Serrano J**, **Zang T**, **Bieniasz PD**. 2001. HIV-1 and Ebola virus encode
906 small peptide motifs that recruit Tsg101 to sites of particle assembly to facilitate
907 egress. Nat Med **7**:1313–1319.

908 32. **Martin-Serrano J**, **Zang T**, **Bieniasz PD**. 2003. Role of ESCRT-I in retroviral
909 budding. J Virol **77**:4794–4804.

910 33. **Popov S**, **Popova E**, **Inoue M**, **Göttlinger HG**. 2008. Human immunodeficiency
911 virus type 1 Gag engages the Bro1 domain of ALIX/AIP1 through the
912 nucleocapsid. J Virol **82**:1389–1398.

913 34. **Chen J**, **Nikolaitchik O**, **Singh J**, **Wright A**, **Bencsics CE**, **Coffin JM**, **Ni N**,
914 **Lockett S**, **Pathak VK**, **Hu W-S**. 2009. High efficiency of HIV-1 genomic RNA
915 packaging and heterozygote formation revealed by single virion analysis. Proc
916 Natl Acad Sci U S A **106**:13535–13540.

917 35. **Moore MD**, **Nikolaitchik OA**, **Chen J**, **Hammarskjöld M-L**, **Rekosh D**, **Hu W-S**.
918 2009. Probing the HIV-1 genomic RNA trafficking pathway and dimerization by
919 genetic recombination and single virion analyses. PLoS Pathog **5**:e1000627.

920 36. **Nikolaitchik OA**, **Dilley KA**, **Fu W**, **Gorelick RJ**, **Tai S-HS**, **Soheilian F**, **Ptak**
921 **RG**, **Nagashima K**, **Pathak VK**, **Hu W-S**. 2013. Dimeric RNA Recognition
922 Regulates HIV-1 Genome Packaging. PLoS Pathog **9**:e1003249.

923 37. **Lever A**, **Gottlinger H**, **Haseltine W**, **Sodroski J**. 1989. Identification of a
924 sequence required for efficient packaging of human immunodeficiency virus type
925 1 RNA into virions. J Virol **63**:4085–4087.

926 38. **Zhang Y**, **Barklis E**. 1995. Nucleocapsid protein effects on the specificity of
927 retrovirus RNA encapsidation. J Virol **69**:5716–5722.

928 39. **Kutluay SB**, **Zang T**, **Blanco-Melo D**, **Powell C**, **Jannain D**, **Errando M**,
929 **Bieniasz PD**. 2014. Global changes in the RNA binding specificity of HIV-1 gag
930 regulate virion genesis. Cell **159**:1096–1109.

931 40. **Didierlaurent L**, **Racine PJ**, **Houzet L**, **Chamontin C**, **Berkhout B**, **Mougel M**.
932 2011. Role of HIV-1 RNA and protein determinants for the selective packaging of
933 spliced and unspliced viral RNA and host U6 and 7SL RNA in virus particles.
934 Nucleic Acids Res **39**:8915–8927.

935 41. **Keene SE**, **Telesnitsky A**. 2012. cis-Acting determinants of 7SL RNA packaging
936 by HIV-1. J Virol **86**:7934–7942.

937 42. **Schopman NCT**, **van Montfort T**, **Willemsen M**, **Knoepfel SA**, **Pollakis G**, **van**
938 **Kampen A**, **Sanders RW**, **Haasnoot J**, **Berkhout B**. 2012. Selective packaging
939 of cellular miRNAs in HIV-1 particles. Virus Res **169**:438–447.

940 43. **Eckwahl MJ**, **Arnion H**, **Kharytonchyk S**, **Zang T**, **Bieniasz PD**, **Telesnitsky A**,
941 **Wolin SL**. 2016. Analysis of the human immunodeficiency virus-1 RNA
942 packageome. RNA N Y N.

943 44. **Purohit P**, **Dupont S**, **Stevenson M**, **Green MR**. 2001. Sequence-specific
944 interaction between HIV-1 matrix protein and viral genomic RNA revealed by in
945 vitro genetic selection. RNA N Y N **7**:576–584.

946 45. **Chukkapalli V**, **Hogue IB**, **Boyko V**, **Hu W-S**, **Ono A**. 2008. Interaction between
947 the human immunodeficiency virus type 1 Gag matrix domain and
948 phosphatidylinositol-(4,5)-bisphosphate is essential for efficient gag membrane
949 binding. J Virol **82**:2405–2417.

950 46. **Chukkapalli V**, **Oh SJ**, **Ono A**. 2010. Opposing mechanisms involving RNA and
951 lipids regulate HIV-1 Gag membrane binding through the highly basic region of
952 the matrix domain. Proc Natl Acad Sci U S A **107**:1600–1605.

953 47. **Swanson CM**, **Malim MH**. 2006. Retrovirus RNA trafficking: from chromatin to
954 invasive genomes. Traffic Cph Den **7**:1440–1450.

955 48. **Cochrane AW**, **McNally MT**, **Mouland AJ**. 2006. The retrovirus RNA trafficking
956 granule: from birth to maturity. Retrovirology **3**:18.

957 49. **Lingappa JR**, **Reed JC**, **Tanaka M**, **Chutiraka K**, **Robinson BA**. 2014. How HIV-
958 1 Gag assembles in cells: Putting together pieces of the puzzle. Virus Res.

959 50. **Chen J**, **Grunwald D**, **Sardo L**, **Galli A**, **Plisov S**, **Nikolaitchik OA**, **Chen D**,
960 **Lockett S**, **Larson DR**, **Pathak VK**, **Hu W-S**. 2014. Cytoplasmic HIV-1 RNA is
961 mainly transported by diffusion in the presence or absence of Gag protein. Proc
962 Natl Acad Sci U S A.

963 51. **Basyuk E**, **Galli T**, **Mougel M**, **Blanchard J-M**, **Sitbon M**, **Bertrand E**. 2003.
964 Retroviral genomic RNAs are transported to the plasma membrane by endosomal
965 vesicles. Dev Cell **5**:161–174.

966 52. **Poole E**, **Strappe P**, **Mok H-P**, **Hicks R**, **Lever AML**. 2005. HIV-1 Gag-RNA
967 interaction occurs at a perinuclear/centrosomal site; analysis by confocal
968 microscopy and FRET. Traffic Cph Den **6**:741–755.

969 53. **Lehmann M**, **Milev MP**, **Abrahamyan L**, **Yao X-J**, **Pante N**, **Mouland AJ**. 2009.
970 Intracellular transport of human immunodeficiency virus type 1 genomic RNA and
971 viral production are dependent on dynein motor function and late endosome
972 positioning. J Biol Chem **284**:14572–14585.

973 54. **Perez-Caballero D**, **Hatziioannou T**, **Martin-Serrano J**, **Bieniasz PD**. 2004.
974 Human immunodeficiency virus type 1 matrix inhibits and confers cooperativity on
975 gag precursor-membrane interactions. J Virol **78**:9560–9563.

976 55. **Göttlinger HG**, **Sodroski JG**, **Haseltine WA**. 1989. Role of capsid precursor
977 processing and myristoylation in morphogenesis and infectivity of human
978 immunodeficiency virus type 1. Proc Natl Acad Sci U S A **86**:5781–5785.

979 56. **Hermida-Matsumoto L**, **Resh MD**. 1999. Human immunodeficiency virus type 1
980 protease triggers a myristoyl switch that modulates membrane binding of
981 Pr55(gag) and p17MA. J Virol **73**:1902–1908.

982 57. **Li H**, **Dou J**, **Ding L**, **Spearman P**. 2007. Myristoylation is required for human
983 immunodeficiency virus type 1 Gag-Gag multimerization in mammalian cells. J
984 Virol **81**:12899–12910.

985 58. **Chen J**, **Rahman SA**, **Nikolaitchik OA**, **Grunwald D**, **Sardo L**, **Burdick RC**,
986 **Plisov S**, **Liang E**, **Tai S**, **Pathak VK**, **Hu W-S**. 2016. HIV-1 RNA genome
987 dimerizes on the plasma membrane in the presence of Gag protein. Proc Natl
988 Acad Sci U S A **113**:E201–208.

989 59. **Jouvenet N**, **Simon SM**, **Bieniasz PD**. 2009. Imaging the interaction of HIV-1
990 genomes and Gag during assembly of individual viral particles. Proc Natl Acad Sci
991 U S A **106**:19114–19119.

992 60. **Ivanchenko S**, **Godinez WJ**, **Lampe M**, **Kräusslich H-G**, **Eils R**, **Rohr K**,
993 **Bräuchle C**, **Müller B**, **Lamb DC**. 2009. Dynamics of HIV-1 assembly and
994 release. PLoS Pathog **5**:e1000652.

995 61. **Ku P-I**, **Miller AK**, **Ballew J**, **Sandrin V**, **Adler FR**, **Saffarian S**. 2013.
996 Identification of Pauses during Formation of HIV-1 Virus Like Particles. Biophys J
997 **105**:2262–2272.

998 62. **Sardo L**, **Hatch SC**, **Chen J**, **Nikolaitchik O**, **Burdick RC**, **Chen D**, **Westlake**
999 **CJ**, **Lockett S**, **Pathak VK**, **Hu W-S**. 2015. The Dynamics of HIV-1 RNA Near the
1000 Plasma Membrane During Virus Assembly. J Virol.

1001 63. **Schwartz S**, **Campbell M**, **Nasioulas G**, **Harrison J**, **Felber BK**, **Pavlakis GN**.
1002 1992. Mutational inactivation of an inhibitory sequence in human

1003 immunodeficiency virus type 1 results in Rev-independent gag expression. J Virol
1004 **66**:7176–7182.

1005 64. **Naldini L**, **Blömer U**, **Gallay P**, **Ory D**, **Mulligan R**, **Gage FH**, **Verma IM**, **Trono**
1006 **D**. 1996. In vivo gene delivery and stable transduction of nondividing cells by a
1007 lentiviral vector. Science **272**:263–267.

1008 65. **Kotsopoulou E**, **Kim VN**, **Kingsman AJ**, **Kingsman SM**, **Mitrophanous KA**.
1009 2000. A Rev-independent human immunodeficiency virus type 1 (HIV-1)-based
1010 vector that exploits a codon-optimized HIV-1 gag-pol gene. J Virol **74**:4839–4852.

1011 66. **Swanson CM**, **Puffer BA**, **Ahmad KM**, **Doms RW**, **Malim MH**. 2004. Retroviral
1012 mRNA nuclear export elements regulate protein function and virion assembly.
1013 EMBO J **23**:2632–2640.

1014 67. **Jin J**, **Sturgeon T**, **Chen C**, **Watkins SC**, **Weisz OA**, **Montelaro RC**. 2007.
1015 Distinct intracellular trafficking of equine infectious anemia virus and human
1016 immunodeficiency virus type 1 Gag during viral assembly and budding revealed
1017 by bimolecular fluorescence complementation assays. J Virol **81**:11226–11235.

1018 68. **Jin J**, **Sturgeon T**, **Weisz OA**, **Mothes W**, **Montelaro RC**. 2009. HIV-1 matrix
1019 dependent membrane targeting is regulated by Gag mRNA trafficking. PloS One
1020 **4**:e6551.

1021 69. **Sherer NM**, **Swanson CM**, **Papaioannou S**, **Malim MH**. 2009. Matrix mediates
1022 the functional link between human immunodeficiency virus type 1 RNA nuclear

export elements and the assembly competency of Gag in murine cells. J Virol **83**:8525–8535.

70. **Malim MH**, **Cullen BR**. 1993. Rev and the fate of pre-mRNA in the nucleus: implications for the regulation of RNA processing in eukaryotes. Mol Cell Biol **13**:6180–6189.

71. **Hope TJ**. 1997. Viral RNA export. Chem Biol **4**:335–344.

72. **Cullen BR**. 2003. Nuclear mRNA export: insights from virology. Trends Biochem Sci **28**:419–424.

73. **Malim MH**, **Hauber J**, **Fenrick R**, **Cullen BR**. 1988. Immunodeficiency virus rev trans-activator modulates the expression of the viral regulatory genes. Nature **335**:181–183.

74. **Malim MH**, **Tiley LS**, **McCarn DF**, **Rusche JR**, **Hauber J**, **Cullen BR**. 1990. HIV-1 structural gene expression requires binding of the Rev trans-activator to its RNA target sequence. Cell **60**:675–683.

75. **Sherer NM**, **Swanson CM**, **Hué S**, **Roberts RG**, **Bergeron JRC**, **Malim MH**. 2011. Evolution of a species-specific determinant within human CRM1 that regulates the post-transcriptional phases of HIV-1 replication. PLoS Pathog **7**:e1002395.

76. **Bray M**, **Prasad S**, **Dubay JW**, **Hunter E**, **Jeang KT**, **Rekosh D**, **Hammarskjöld ML**. 1994. A small element from the Mason-Pfizer monkey virus genome makes

human immunodeficiency virus type 1 expression and replication Rev-independent. Proc Natl Acad Sci U S A **91**:1256–1260.

77. **Ernst RK**, **Bray M**, **Rekosh D**, **Hammarskjöld ML**. 1997. A structured retroviral RNA element that mediates nucleocytoplasmic export of intron-containing RNA. Mol Cell Biol **17**:135–144.

78. **Pasquinelli AE**, **Ernst RK**, **Lund E**, **Grimm C**, **Zapp ML**, **Rekosh D**, **Hammarskjöld ML**, **Dahlberg JE**. 1997. The constitutive transport element (CTE) of Mason-Pfizer monkey virus (MPMV) accesses a cellular mRNA export pathway. EMBO J **16**:7500–7510.

79. **Rizvi TA**, **Schmidt RD**, **Lew KA**. 1997. Mason-Pfizer monkey virus (MPMV) constitutive transport element (CTE) functions in a position-dependent manner. Virology **236**:118–129.

80. **Pessel-Vivares L**, **Ferrer M**, **Lainé S**, **Mougel M**. 2014. MLV requires Tap/NXF1-dependent pathway to export its unspliced RNA to the cytoplasm and to express both spliced and unspliced RNAs. Retrovirology **11**:21.

81. **Pocock GM**, **Becker JT**, **Swanson CM**, **Ahlquist P**, **Sherer NM**. 2016. HIV-1 and M-PMV RNA Nuclear Export Elements Program Viral Genomes for Distinct Cytoplasmic Trafficking Behaviors. PLoS Pathog **12**:e1005565.

82. **Adachi A**, **Gendelman HE**, **Koenig S**, **Folks T**, **Willey R**, **Rabson A**, **Martin MA**. 1986. Production of acquired immunodeficiency syndrome-associated retrovirus in

human and nonhuman cells transfected with an infectious molecular clone. J Virol **59**:284–291.

83. **Aligeti M**, **Behrens RT**, **Pocock GM**, **Schindelin J**, **Dietz C**, **Eliceiri KW**, **Swanson CM**, **Malim MH**, **Ahlquist P**, **Sherer NM**. 2014. Cooperativity Among Rev-Associated Nuclear Export Signals Regulates HIV-1 Gene Expression and is a Determinant of Virus Species Tropism. J Virol.

84. **Hermida-Matsumoto L**, **Resh MD**. 2000. Localization of human immunodeficiency virus type 1 Gag and Env at the plasma membrane by confocal imaging. J Virol **74**:8670–8679.

85. **Subach OM**, **Cranfill PJ**, **Davidson MW**, **Verkhusha VV**. 2011. An Enhanced Monomeric Blue Fluorescent Protein with the High Chemical Stability of the Chromophore. PLoS ONE **6**:e28674.

86. **Swanson CM**, **Sherer NM**, **Malim MH**. 2010. SRp40 and SRp55 promote the translation of unspliced human immunodeficiency virus type 1 RNA. J Virol **84**:6748–6759.

87. **Swanson CM**, **Puffer BA**, **Ahmad KM**, **Doms RW**, **Malim MH**. 2004. Retroviral mRNA nuclear export elements regulate protein function and virion assembly. EMBO J **23**:2632–2640.

88. **Femino AM**, **Fay FS**, **Fogarty K**, **Singer RH**. 1998. Visualization of single RNA transcripts in situ. Science **280**:585–590.

89. **Sigal CT**, **Zhou W**, **Buser CA**, **McLaughlin S**, **Resh MD**. 1994. Amino-terminal basic residues of Src mediate membrane binding through electrostatic interaction with acidic phospholipids. Proc Natl Acad Sci U S A **91**:12253–12257.

90. **Kalderon D**, **Roberts BL**, **Richardson WD**, **Smith AE**. 1984. A short amino acid sequence able to specify nuclear location. Cell **39**:499–509.

91. **Sheehy AM**, **Gaddis NC**, **Choi JD**, **Malim MH**. 2002. Isolation of a human gene that inhibits HIV-1 infection and is suppressed by the viral Vif protein. Nature **418**:646–650.

92. **Chesebro B**, **Wehrly K**, **Nishio J**, **Perryman S**. 1992. Macrophage-tropic human immunodeficiency virus isolates from different patients exhibit unusual V3 envelope sequence homogeneity in comparison with T-cell-tropic isolates: definition of critical amino acids involved in cell tropism. J Virol **66**:6547–6554.

93. **Raj A**, **van den Bogaard P**, **Rifkin SA**, **van Oudenaarden A**, **Tyagi S**. 2008. Imaging individual mRNA molecules using multiple singly labeled probes. Nat Methods **5**:877–879.

94. **Chou Y**, **Heaton NS**, **Gao Q**, **Palese P**, **Singer RH**, **Singer R**, **Lionnet T**. 2013. Colocalization of different influenza viral RNA segments in the cytoplasm before viral budding as shown by single-molecule sensitivity FISH analysis. PLoS Pathog **9**:e1003358.

95. **Schindelin J**, **Arganda-Carreras I**, **Frise E**, **Kaynig V**, **Longair M**, **Pietzsch T**, **Preibisch S**, **Rueden C**, **Saalfeld S**, **Schmid B**, **Tinevez J-Y**, **White DJ**,

Hartenstein V, **Eliceiri K**, **Tomancak P**, **Cardona A**. 2012. Fiji: an open-source platform for biological-image analysis. Nat Methods **9**:676–682.

96. **Buck CB**, **Shen X**, **Egan MA**, **Pierson TC**, **Walker CM**, **Siliciano RF**. 2001. The human immunodeficiency virus type 1 gag gene encodes an internal ribosome entry site. J Virol **75**:181–191.

97. **Poon DTK**, **Chertova EN**, **Ott DE**. 2002. Human immunodeficiency virus type 1 preferentially encapsidates genomic RNAs that encode Pr55(Gag): functional linkage between translation and RNA packaging. Virology **293**:368–378.

98. **Dykeman EC**, **Stockley PG**, **Twarock R**. 2014. Solving a Levinthal's paradox for virus assembly identifies a unique antiviral strategy. Proc Natl Acad Sci U S A **111**:5361–5366.

99. **Patel N**, **Dykeman EC**, **Coutts RHA**, **Lomonossoff GP**, **Rowlands DJ**, **Phillips SEV**, **Ranson N**, **Twarock R**, **Tuma R**, **Stockley PG**. 2015. Revealing the density of encoded functions in a viral RNA. Proc Natl Acad Sci 201420812.

100. **Stockley PG**, **White SJ**, **Dykeman E**, **Manfield I**, **Rolfsson O**, **Patel N**, **Bingham R**, **Barker A**, **Wroblewski E**, **Chandler-Bostock R**, **Weiß EU**, **Ranson NA**, **Tuma R**, **Twarock R**. 2016. Bacteriophage MS2 genomic RNA encodes an assembly instruction manual for its capsid. Bacteriophage **6**:e1157666.

101. **Rolfsson Ó**, **Middleton S**, **Manfield IW**, **White SJ**, **Fan B**, **Vaughan R**, **Ranson NA**, **Dykeman E**, **Twarock R**, **Ford J**, **Cheng Kao C**, **Stockley PG**. 2016. Direct

1124 Evidence for Packaging Signal-Mediated Assembly of Bacteriophage MS2. J Mol
1125 Biol **428**:431–448.

1126 102. **Yang J**, **Bogerd HP**, **Wang PJ**, **Page DC**, **Cullen BR**. 2001. Two closely related
1127 human nuclear export factors utilize entirely distinct export pathways. Mol Cell
1128 **8**:397–406.

1129 103. **Wiegand HL**, **Coburn GA**, **Zeng Y**, **Kang Y**, **Bogerd HP**, **Cullen BR**. 2002.
1130 Formation of Tap/NXT1 heterodimers activates Tap-dependent nuclear mRNA
1131 export by enhancing recruitment to nuclear pore complexes. Mol Cell Biol **22**:245–
1132 256.

1133 104. **Jolly C**, **Kashefi K**, **Hollinshead M**, **Sattentau QJ**. 2004. HIV-1 Cell to Cell
1134 Transfer across an Env-induced, Actin-dependent Synapse. J Exp Med **199**:283–
1135 293.

1136 105. **Sasaki H**, **Ozaki H**, **Karaki H**, **Nonomura Y**. 2004. Actin filaments play an
1137 essential role for transport of nascent HIV-1 proteins in host cells. Biochem
1138 Biophys Res Commun **316**:588–593.

1139 106. **Jolly C**, **Mitar I**, **Sattentau QJ**. 2007. Requirement for an Intact T-Cell Actin and
1140 Tubulin Cytoskeleton for Efficient Assembly and Spread of Human
1141 Immunodeficiency Virus Type 1. J Virol **81**:5547–5560.

1142 107. **Cooper J**, **Liu L**, **Woodruff EA**, **Taylor HE**, **Goodwin JS**, **D'Aquila RT**,
1143 **Spearman P**, **Hildreth JEK**, **Dong X**. 2011. Filamin A protein interacts with

1144 human immunodeficiency virus type 1 Gag protein and contributes to productive
1145 particle assembly. J Biol Chem **286**:28498–28510.

1146 108. **Wen X**, **Ding L**, **Hunter E**, **Spearman P**. 2014. An siRNA screen of membrane
1147 trafficking genes highlights pathways common to HIV-1 and M-PMV virus
1148 assembly and release. PloS One **9**:e106151.

1149 109. **Wen X**, **Ding L**, **Wang J-J**, **Qi M**, **Hammonds J**, **Chu H**, **Chen X**, **Hunter E**,
1150 **Spearman P**. 2014. ROCK1 and LIM kinase modulate retrovirus particle release
1151 and cell-cell transmission events. J Virol **88**:6906–6921.

1152 110. **Ott DE**, **Coren LV**, **Kane BP**, **Busch LK**, **Johnson DG**, **Sowder RC**, **Chertova**
1153 **EN**, **Arthur LO**, **Henderson LE**. 1996. Cytoskeletal proteins inside human
1154 immunodeficiency virus type 1 virions. J Virol **70**:7734–7743.

1155 111. **Thomas A**, **Mariani-Floderer C**, **López-Huertas MR**, **Gros N**, **Hamard-Péron E**,
1156 **Favard C**, **Ohlmann T**, **Alcamí J**, **Muriaux D**. 2015. Involvement of the Rac1-
1157 IRSp53-Wave2-Arp2/3 Signaling Pathway in HIV-1 Gag Particle Release in CD4
1158 T Cells. J Virol **89**:8162–8181.

1159 112. **Riedl J**, **Crevenna AH**, **Kessenbrock K**, **Yu JH**, **Neukirchen D**, **Bista M**, **Bradke**
1160 **F**, **Jenne D**, **Holak TA**, **Werb Z**, **Sixt M**, **Wedlich-Soldner R**. 2008. Lifeact: a
1161 versatile marker to visualize F-actin. Nat Methods **5**:605–607.

1162 113. **Saad JS**, **Loeliger E**, **Luncsford P**, **Liriano M**, **Tai J**, **Kim A**, **Miller J**, **Joshi A**,
1163 **Freed EO**, **Summers MF**. 2007. Point mutations in the HIV-1 matrix protein turn
1164 off the myristyl switch. J Mol Biol **366**:574–585.

114. **Bleck M**, **Itano MS**, **Johnson DS**, **Thomas VK**, **North AJ**, **Bieniasz PD**, **Simon SM**. 2014. Temporal and spatial organization of ESCRT protein recruitment during HIV-1 budding. Proc Natl Acad Sci U S A.

115. **Morikawa Y**, **Hockley DJ**, **Nermut MV**, **Jones IM**. 2000. Roles of matrix, p2, and N-terminal myristoylation in human immunodeficiency virus type 1 Gag assembly. J Virol **74**:16–23.

116. **Briggs JAG**, **Wilk T**, **Welker R**, **Kräusslich H-G**, **Fuller SD**. 2003. Structural organization of authentic, mature HIV-1 virions and cores. EMBO J **22**:1707–1715.

117. **Benjamin J**, **Ganser-Pornillos BK**, **Tivol WF**, **Sundquist WI**, **Jensen GJ**. 2005. Three-dimensional structure of HIV-1 virus-like particles by electron cryotomography. J Mol Biol **346**:577–588.

118. **Datta SAK**, **Temeselew LG**, **Crist RM**, **Soheilian F**, **Kamata A**, **Mirro J**, **Harvin D**, **Nagashima K**, **Cachau RE**, **Rein A**. 2011. On the role of the SP1 domain in HIV-1 particle assembly: a molecular switch? J Virol **85**:4111–4121.

119. **Datta SAK**, **Clark PK**, **Fan L**, **Ma B**, **Harvin DP**, **Sowder RC**, **Nussinov R**, **Wang Y-X**, **Rein A**. 2015. Dimerization of the SP1 Region of HIV-1 Gag Induces a Helical Conformation and Association into Helical Bundles: Implications for Particle Assembly. J Virol **90**:1773–1787.

120. **Ward AM**, **Rekosh D**, **Hammarskjold M-L**. 2009. Trafficking through the Rev/RRE pathway is essential for efficient inhibition of human immunodeficiency

virus type 1 by an antisense RNA derived from the envelope gene. J Virol **83**:940–952.

121. **Groom HCT**, **Anderson EC**, **Dangerfield JA**, **Lever AML**. 2009. Rev regulates translation of human immunodeficiency virus type 1 RNAs. J Gen Virol **90**:1141–1147.

122. **Brandt S**, **Blissenbach M**, **Grewe B**, **Konietzny R**, **Grunwald T**, **Uberla K**. 2007. Rev proteins of human and simian immunodeficiency virus enhance RNA encapsidation. PLoS Pathog **3**:e54.

123. **Grewe B**, **Uberla K**. 2010. The human immunodeficiency virus type 1 Rev protein: ménage à trois during the early phase of the lentiviral replication cycle. J Gen Virol **91**:1893–1897.

124. **Bolinger C**, **Boris-Lawrie K**. 2009. Mechanisms employed by retroviruses to exploit host factors for translational control of a complicated proteome. Retrovirology **6**:8.

125. **Arrigo SJ**, **Chen IS**. 1991. Rev is necessary for translation but not cytoplasmic accumulation of HIV-1 vif, vpr, and env/vpu 2 RNAs. Genes Dev **5**:808–819.

126. **D'Agostino DM**, **Felber BK**, **Harrison JE**, **Pavlakis GN**. 1992. The Rev protein of human immunodeficiency virus type 1 promotes polysomal association and translation of gag/pol and vpu/env mRNAs. Mol Cell Biol **12**:1375–1386.

127. **Diaz-Griffero F**, **Taube R**, **Muehlbauer SM**, **Brojatsch J**. 2008. Efficient production of HIV-1 viral-like particles in mouse cells. Biochem Biophys Res Commun **368**:463–469.

128. **Jin J**, **Sturgeon T**, **Weisz OA**, **Mothes W**, **Montelaro RC**. 2009. HIV-1 matrix dependent membrane targeting is regulated by Gag mRNA trafficking. PloS One **4**:e6551.

129. **Jin J**, **Sturgeon T**, **Chen C**, **Watkins SC**, **Weisz OA**, **Montelaro RC**. 2007. Distinct intracellular trafficking of equine infectious anemia virus and human immunodeficiency virus type 1 Gag during viral assembly and budding revealed by bimolecular fluorescence complementation assays. J Virol **81**:11226–11235.

130. **Stake M**, **Singh D**, **Singh G**, **Marcela Hernandez J**, **Kaddis Maldonado R**, **Parent LJ**, **Boris-Lawrie K**. 2015. HIV-1 and two avian retroviral 5' untranslated regions bind orthologous human and chicken RNA binding proteins. Virology **486**:307–320.

131. **Herrera-Carrillo E**, **Berkhout B**. 2015. Bone Marrow Gene Therapy for HIV/AIDS. Viruses **7**:3910–3936.

Figure 1

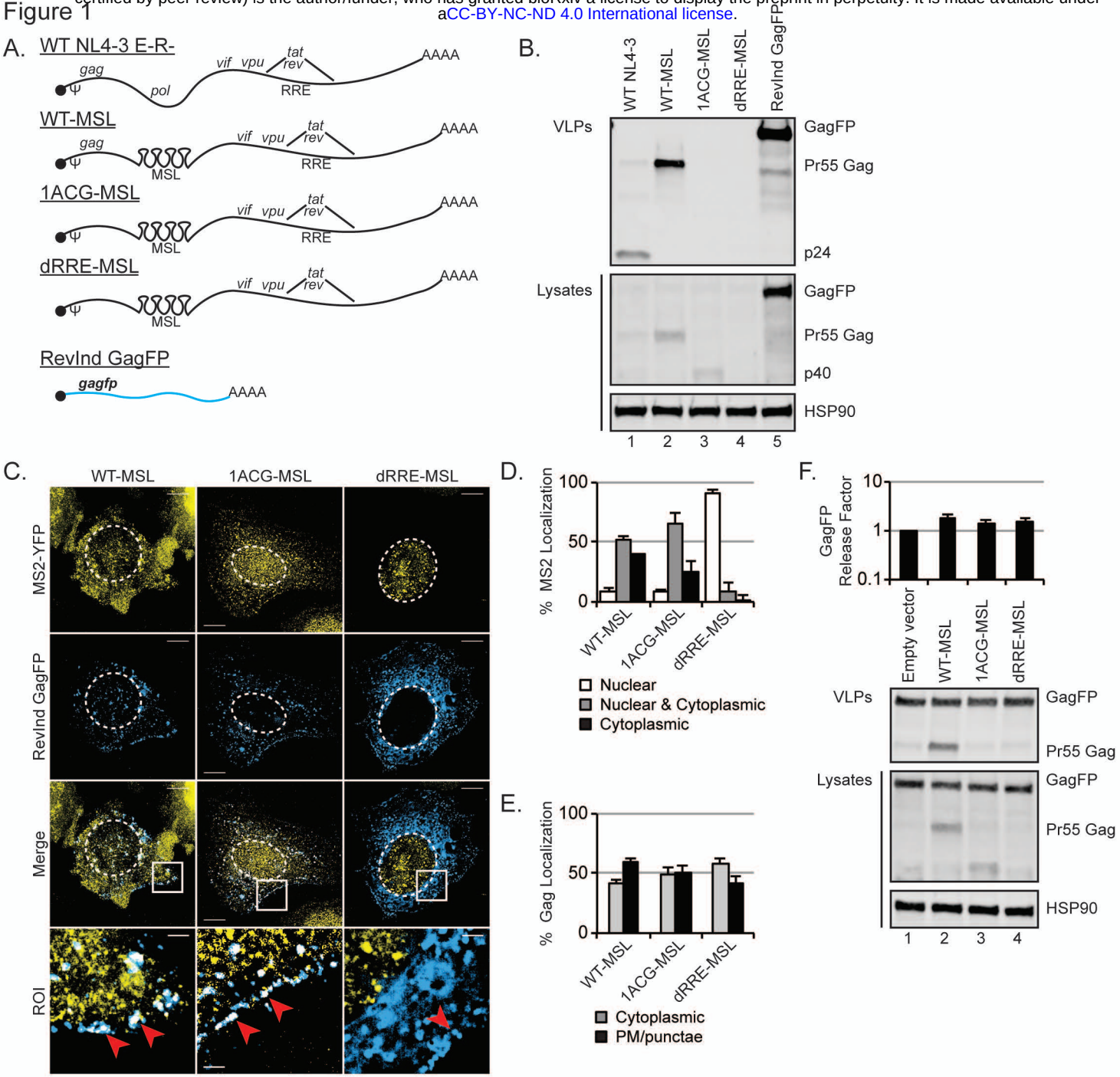

Figure 2

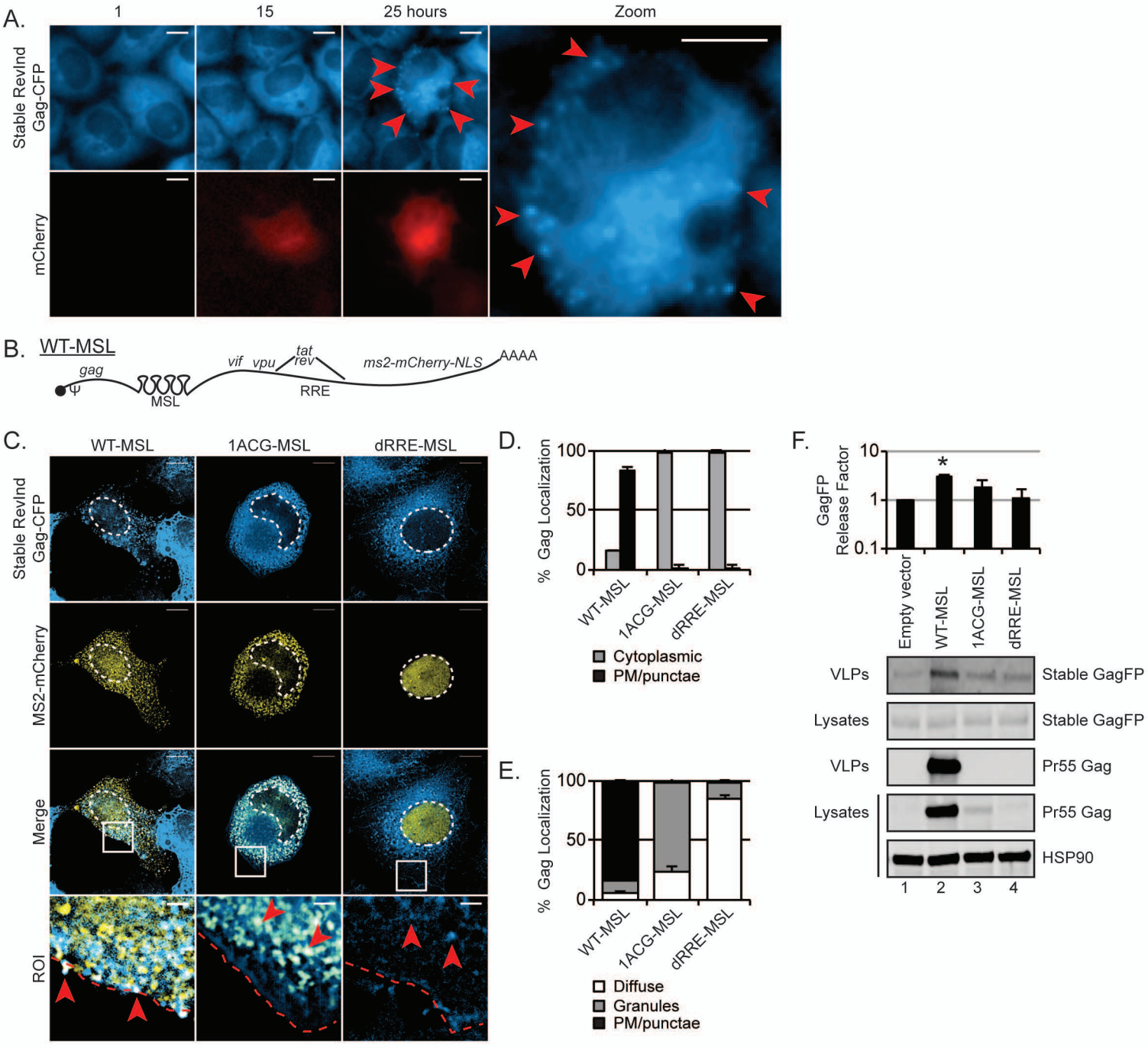

Figure 3

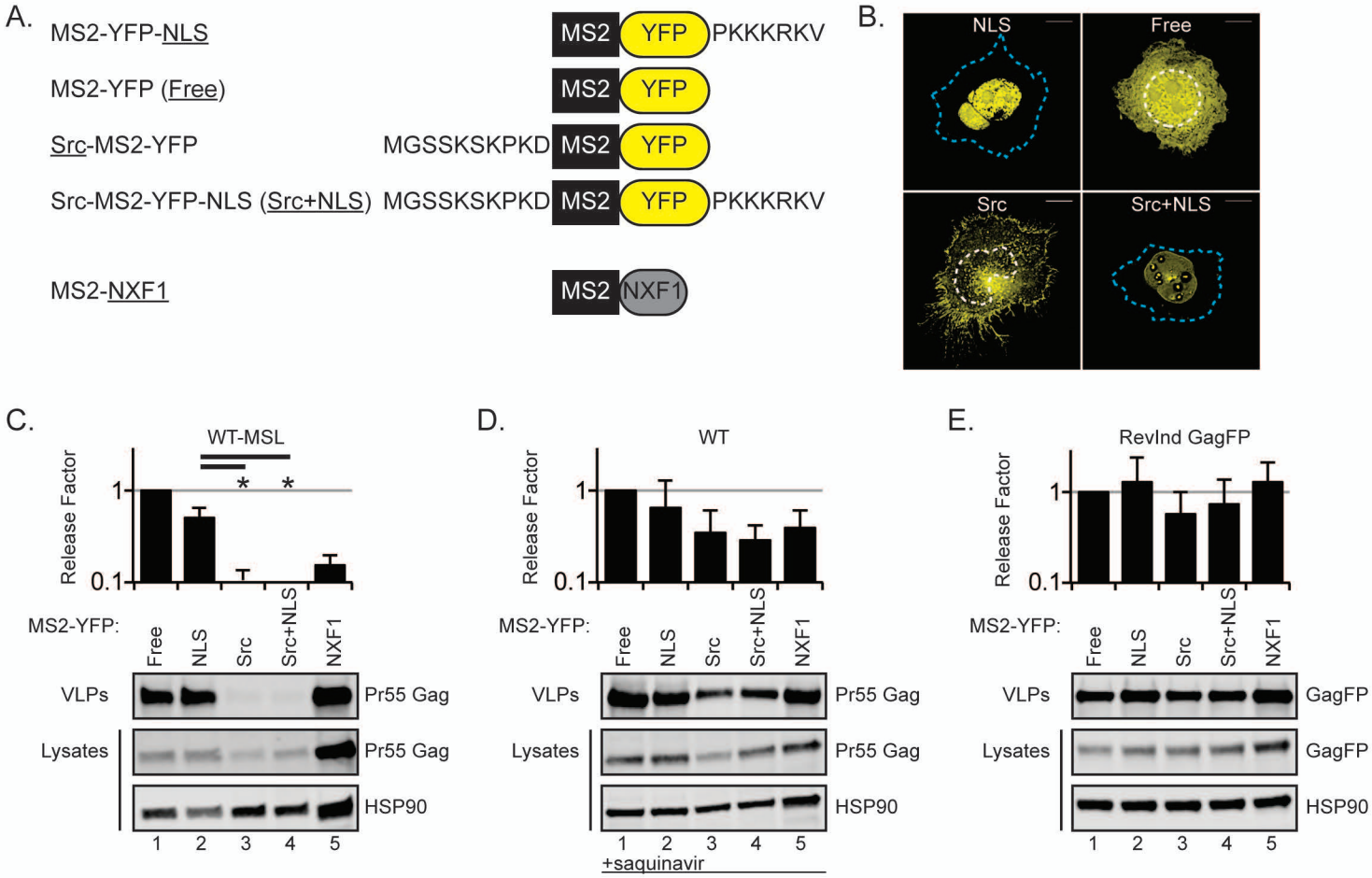

Figure 4

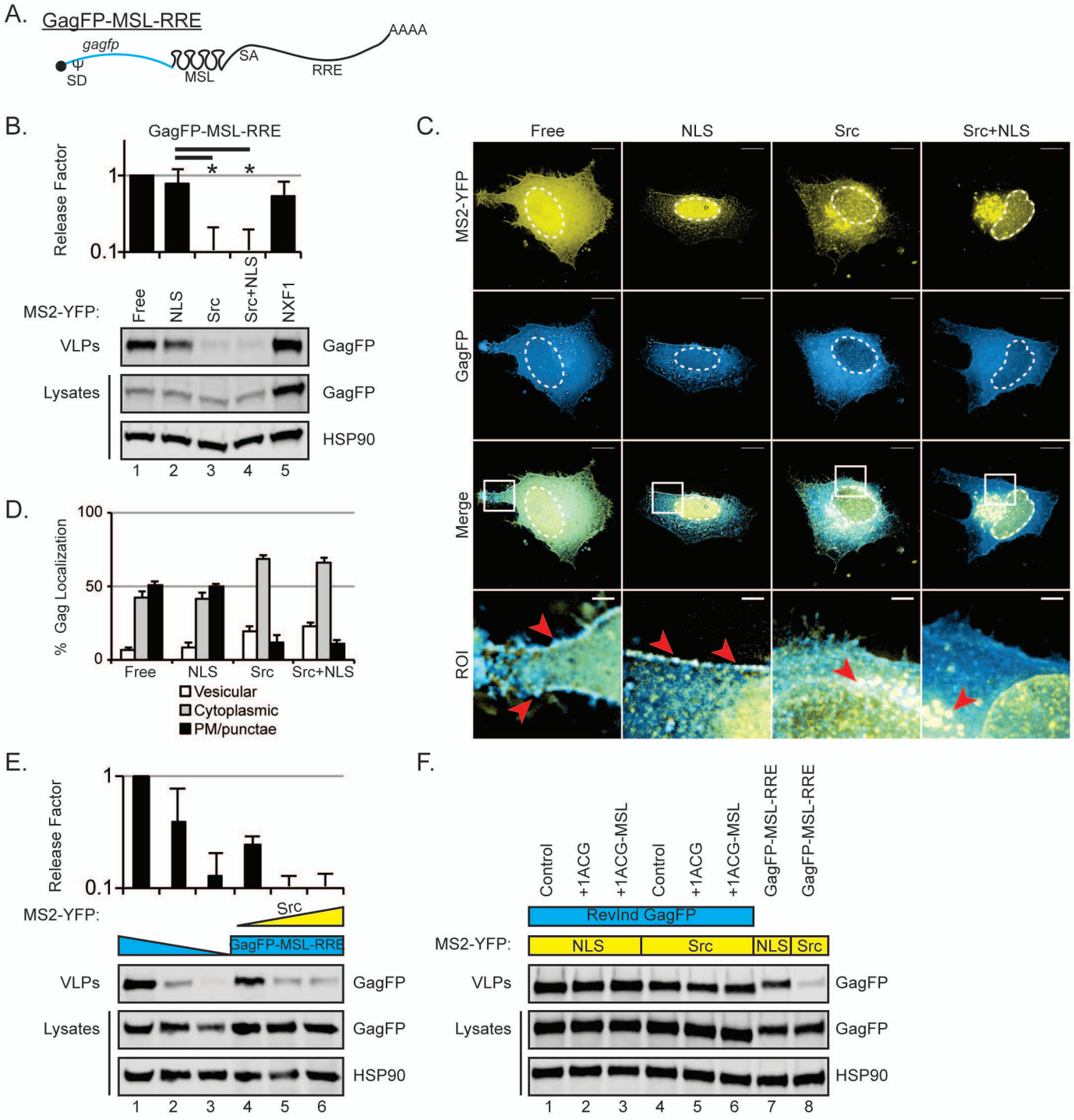

Figure 5

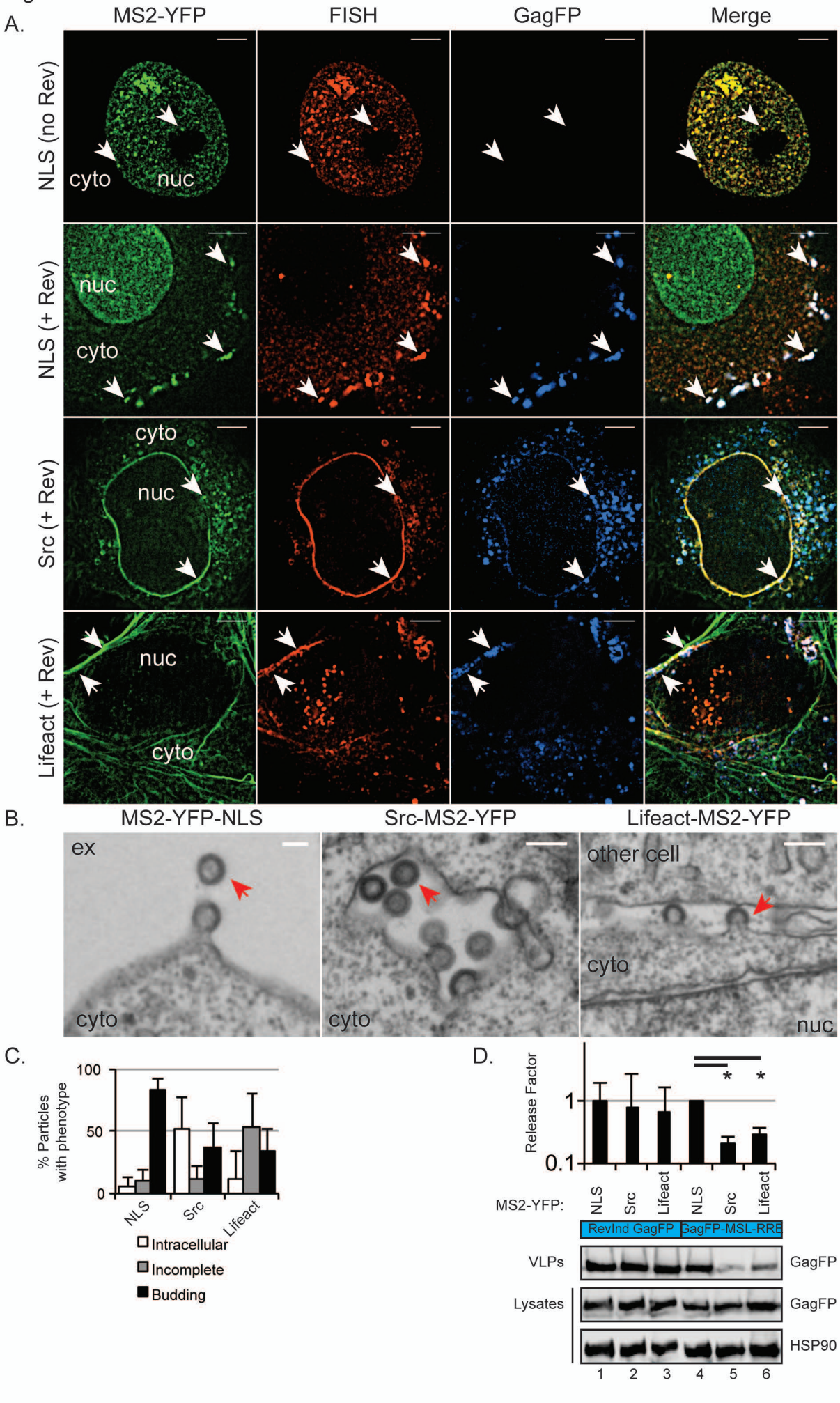

Figure 6

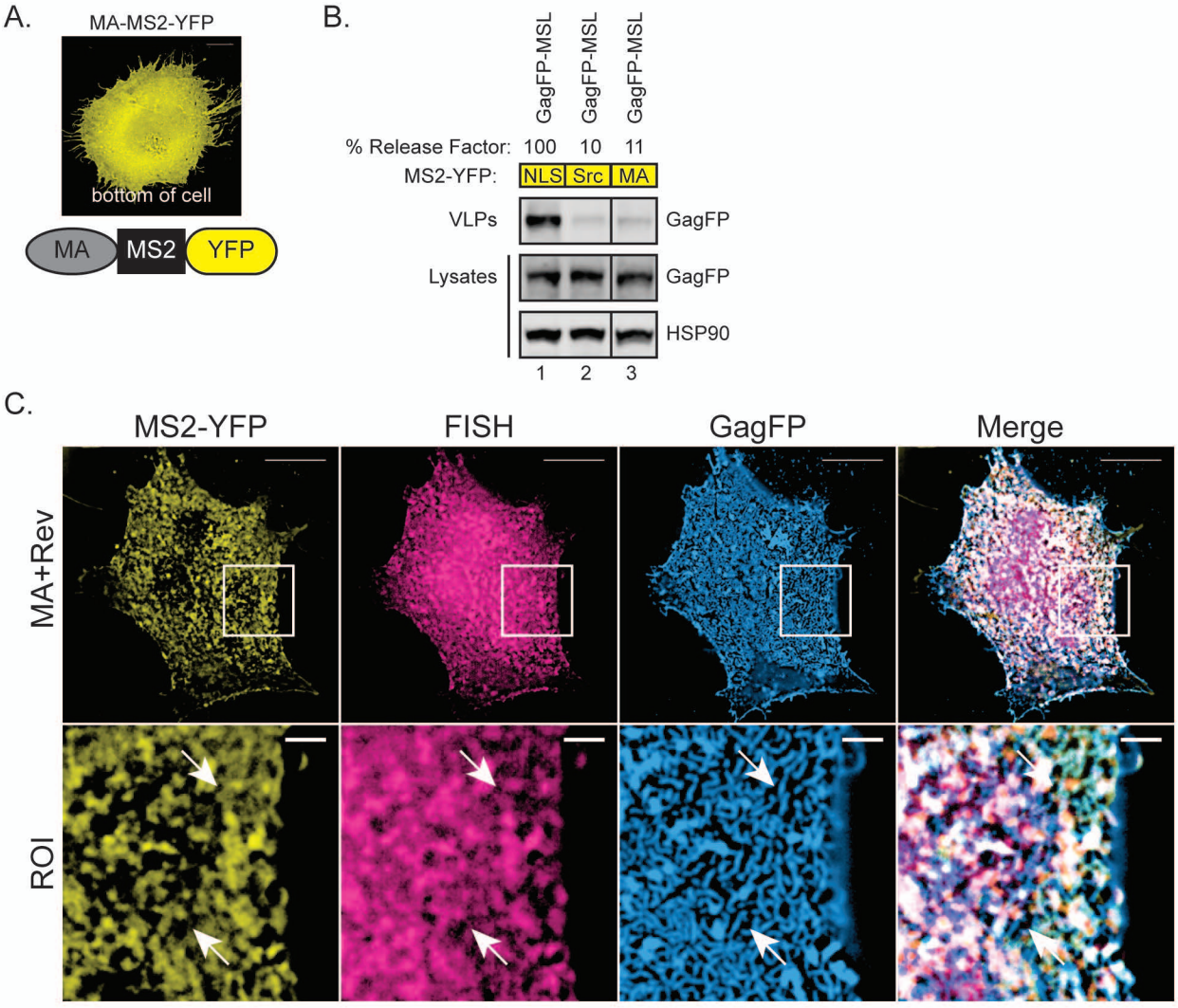

Figure 7

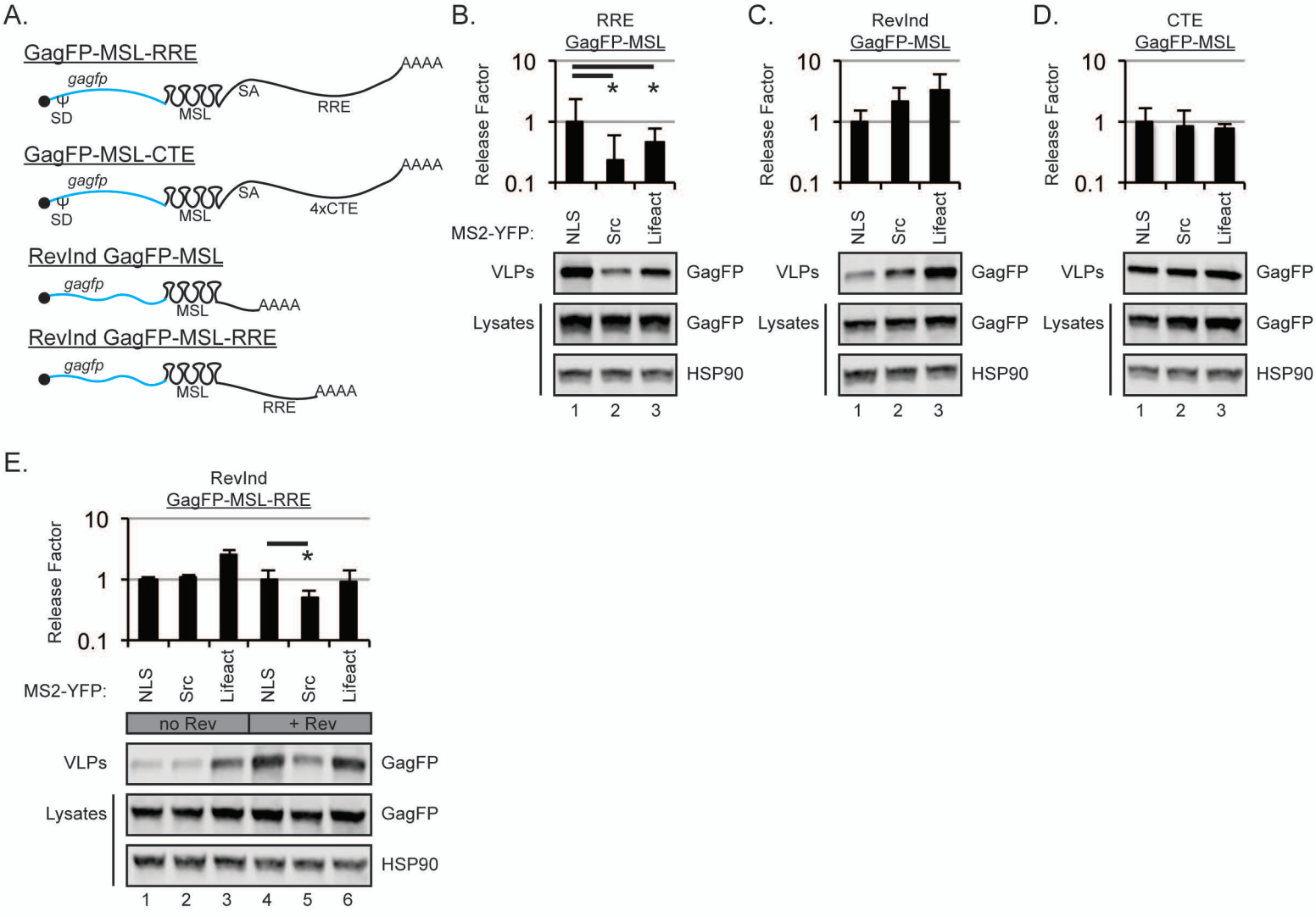

Figure 8

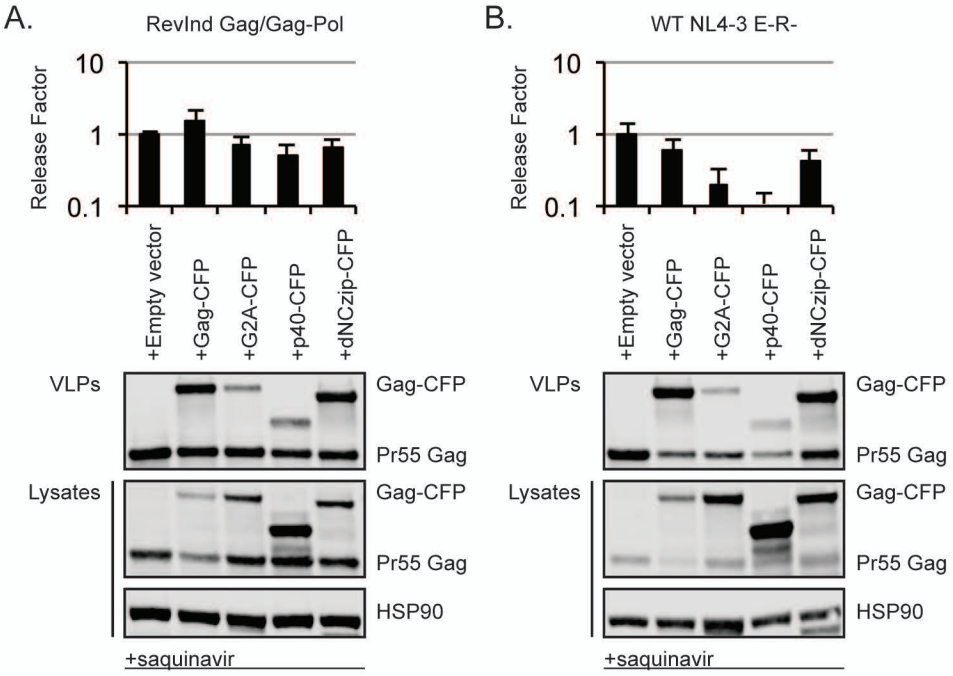

Figure 9